

Z' portal to Chern-Simons Dark Matter

Giorgio Arcadi^{a,*} Pradipta Ghosh^{b,†} Yann Mambrini^{c,‡}

Mathias Pierre^{c,§} and Farinaldo S. Queiroz^{a,¶}

^a*Max Planck Institut für Kernphysik, Saupfercheckweg 1, D-69117 Heidelberg, Germany*

^b*Department of Physics, Vidyasagar College, 39,
Sankar Ghose Lane, Kolkata 700006, India and*

^c*Laboratoire de Physique Théorique, CNRS, Univ. Paris-Sud,
Université Paris-Saclay, 91405 Orsay, France*

We study the phenomenological credibility of a vectorial dark matter, coupled to a Z' portal through Chern-Simons interaction. We scrutinize two possibilities of connecting a Z' with the Standard Model: (1) through kinetic mixing and (2) from a second Chern-Simons interaction. Both scenarios are characterized by suppressed nuclear recoil scatterings, rendering direct detection searches not promising. Indirect detection experiments, on the other hand, furnish complementary limits for TeV scale masses, specially with the CTA. Searches for mono-jet and dileptons signals at the LHC are important to partially probe the kinetic mixing setup. Finally we propose an UV completion of the Chern-Simons Dark Matter framework.

* arcadi@mpi-hd.mpg.de

† tphyspg@gmail.com

‡ yann.mambrini@th.u-psud.fr

§ mathias.pierre@th.u-psud.fr

¶ queiroz@mpi-hd.mpg.de

CONTENTS

I. Introduction	3
II. Scenario-I: Z' - Z interaction via Kinetic mixing	5
A. Dark Matter Phenomenology	8
1. Relic density	8
2. Indirect Detection	10
3. Direct detection	12
B. Collider phenomenology	13
C. Results	15
III. Scenario-II: Z' - Z interaction via a second Chern-Simons term	18
A. The Lagrangian	18
B. Relic density	19
C. Indirect detection	21
D. Direct Detection	21
E. Collider phenomenology	21
F. Results	22
IV. Origin of a Chern-Simons coupling and UV completion	24
V. Summary and Conclusions	28
Acknowledgements	31
A. Decay widths of the Z' boson	32
a. Kinetic mixing scenario	32
b. Two Chern-Simons couplings scenario	32
B. Computation of the Chern-Simons coupling	33
1. Diagrams with two mass insertions : "Chern-Simons" contribution	33
2. Diagrams with axions	36
3. Anomaly cancellation	38
References	40

I. INTRODUCTION

The nature of Dark Matter (DM) remains one of the most exciting and puzzling mysteries of science [1–5] till date. In the context of particle physics it is often assumed that one particle species can account for the entire DM abundance, which is $\sim 27\%$ of the budget of the Universe as indicated by PLANCK [6]. Such a sizable amount of *hitherto undetected matter* has diverse and intricate consequences for various ongoing and near future direct and indirect DM detection experiments [7–20].

The absence of conclusive signals of new physics beyond the Standard Model (SM) concerning the DM leaves a handful of open debate, e.g., what are the particle characteristics of the DM or how they are interacting with the SM particles. A popular solution for the DM puzzle is represented by the Weakly Interacting Massive Particles (WIMPs). In the simplest realization these new particle states, typically scalars or fermions, assumed to be singlet under the SM gauge group, feature interactions with the SM states mediated by the Z or the SM-Higgs boson. Similar theoretical frameworks have also been addressed considering a vectorial DM [21–33]. Unfortunately, such simple models, except for a very few exceptions, are critically challenged by the existing and expected upcoming DM searches from the direct, indirect and collider probes. A detailed overview of these frameworks are addressed recently in ref. [34] (see also ref. [35]).

A natural extension of the above setup is provided by the so called “simplified models” (see ref. [36]) in which the SM mediators are replaced by a new “dark mediator”, of various spin assignments. This dark mediator can be connected to the SM particles by various ways and hence, relates the otherwise secluded DM to the SM particles. However, to ensure elucidate predictions, it is nevertheless necessary to investigate theoretical competence of these simplified setups [37–41], i.e., for example, whether they have consistent unitarity behaviours, reasonable Ultra-Violet (UV) completion and how they can be embedded into unified theory frameworks.

The case of spin-1 mediators, among these setups, perhaps deserves serious attentions as phenomenological study of these frameworks reveals intricate complementary aspects of DM searches with relevant collider observations (see ref. [34] for a thorough discussion). An intriguing origin of such spin-1 mediator(s) can arise as gauge boson(s) of some beyond the SM (BSM) gauge group(s), Abelian or non-Abelian, that simultaneously assigns non-zero gauge charge(s) also for the DM candidate. A spin-1 mediator, maintaining gauge invariance and renormalizability, can couple to the SM Electro-Weak (EW) gauge boson, and thus, subsequently to other SM particles, in a few dif-

ferent ways, ¹ e.g., via a kinetic mixing² [42–45] or using a Chern-Simons (CS) interaction [46–49]. The former can either appear naturally in Lagrangian preserving the gauge invariance and renormalizability of the SM [42, 44, 45] or can get generated after integrating out the heavy fermionic degrees of freedom [42, 43] charged under both the SM and BSM gauge groups. The latter can also arise in an analogous way after integrating out such heavy degrees of freedom, as extensively studied in ref. [50]. The presence of these new fermionic degrees of freedom, if chiral under some representations, introduces new challenges to construct an anomaly free model framework ³. This goal is customarily achieved by arranging anomaly cancellation in the chiral sectors of the theory, by assigning specific couplings/charges for the involved particle species, e.g., by considering distinct couplings between the SM chiral fermions, and possibly also the DM, with the BSM spin-1 mediator as discussed in ref. [51] in the context of unified theories. Some classes of anomalies, like the triangle ones involving Abelian, non-Abelian or a mixture of the two gauge groups can, alternatively be cured through the Green-Schwarz mechanism [52, 53].

In this work we aim to study phenomenological viability of models, consisting of a vectorial DM candidate connected to the SM particles via a Z' -portal [37, 38, 54–73]. We consider specific frameworks that are inspired by Green-Schwarz mechanism (see also refs. [46, 48]), i.e., the connection between the DM and the Z' is mediated by a CS interaction. The vectorial DM can be identified as the cosmologically stable gauge boson of a new BSM symmetry group while the Z' can arise from another BSM Abelian or non-Abelian gauge groups. Confining within the framework of Abelian theory, we will explore two possibilities of how a Z' can coordinate with the SM. These examples, as already mentioned, consider: (1) gauge invariant renormalizable kinetic mixing between the field strength of Z' with $B_{\mu\nu}$, the SM hypercharge field strength and, (2) a second CS interaction involving Z'_μ and the SM hypercharge vector B_μ . For both these scenarios we extensively investigate the impact of measured relic density [6] as well as the existing and anticipated sensitivity reaches from Direct Detection (DD) and Indirect Detection (ID) experiments on the associated model parameter spaces. We also explore relevant theoretical constraints like EW Precision Tests (EWPTs), UV completion etc. for these setups. Finally, for completeness, we also discuss the possible pertinent collider aspects of such models, e.g., invisible Z -decay width, mono- \mathbf{X} , dijets, dilepton searches, etc.

¹ A BSM spin-1 mediator can couple to the SM EW gauge bosons also via the well-known spontaneous symmetry breaking and Higgs mechanism, provided that the SM-Higgs doublet has non-zero charges under the BSM gauge groups. Spontaneous symmetry breaking in the BSM sector is triggered with new SM singlet scalar which may or may not mix with the SM-Higgs. We do not consider this possibility in our analysis.

² A kinetic mixing, from the principle of gauge invariance, is allowed only between the vector bosons of Abelian groups.

³ One can always consider these new fermions to transform vector-like with respect to the SM gauge groups such that no new chiral anomalies appear in the SM.

The paper is organized as follows: in the next two sections we will study phenomenologies of the two aforesaid scenarios relying on the low-energy effective Lagrangians without specifying theoretical issues like UV completion etc. Section IV will be dedicated for this task where we will address the generation of a CS coupling as well as a kinetic mixing in a UV complete setup. We will present the summary of our analyses and put our concluding remarks in Section V. Some useful formulae like detail constructions of an anomaly free model are relegated to the appendices.

II. SCENARIO-I: Z' - Z INTERACTION VIA KINETIC MIXING

In this section we study the aforesaid type-I scenario when the “dark sector”, comprised of a vectorial DM X_μ and a spin-1 vector boson \tilde{V}_μ , is “secluded” from the visible sector, i.e., there exists no direct coupling between this dark sector and the SM fermions⁴. These X_μ and \tilde{V}_μ , for example, can appear as the gauge bosons of some BSM $U(1)_X$ and $U(1)_V$ groups and we consider a CS interaction to connect them together. As already discussed, a bridge between the dark sector and the SM now appears via a kinetic mixing of $\tilde{V}_{\mu\nu}$ and $B_{\mu\nu}$, the field strengths associated with BSM $U(1)_V$ and the SM $U(1)_Y$ gauge group, respectively. A similar kinetic mixing between $X_{\mu\nu}$ and $B_{\mu\nu}$, being renormalizable and allowed by the SM gauge invariance, should also be included in a general Lagrangian. However, we do not consider this possibility for the stability of the DM and postpone further discussion in this direction till section IV.

The relevant phenomenology of the said model can be described by the following low-energy effective Lagrangian:

$$\begin{aligned} \mathcal{L} \supset & -\frac{1}{4}B^{\mu\nu}B_{\mu\nu} - \frac{1}{4}X^{\mu\nu}X_{\mu\nu} - \frac{1}{4}\tilde{V}^{\mu\nu}\tilde{V}_{\mu\nu} - \frac{\sin\delta}{2}\tilde{V}^{\mu\nu}B_{\mu\nu} \\ & +\alpha_{\text{CS}}\epsilon^{\mu\nu\rho\sigma}X_\mu\tilde{V}_\nu X_{\rho\sigma} + \frac{m_V^2}{2}\tilde{V}^\mu\tilde{V}_\mu + \frac{m_X^2}{2}X^\mu X_\mu, \end{aligned} \quad (1)$$

here δ is the kinetic mixing parameter and α_{CS} represents the effective coupling of CS operator. $X_{\mu\nu}$ gives the field strength of $U(1)_X$ group and m_V , m_X represent mass terms of the mediator and the DM. Thus, one gets a set of four free inputs, namely, δ , α_{CS} , m_V and m_X whose ranges will be tested subsequently imposing a series of theoretical and experimental constraints.

The presence of kinetic mixing in eq. (1) implies non-canonical kinetic term for $B_{\mu\nu}$ and also for $\tilde{V}_{\mu\nu}$. In order to generate diagonal kinetic terms in the physical or mass basis one should invoke three different rotations [74–77]. The first rotation, involving then angle δ , takes B_μ , \tilde{V}_μ to a basis (say B_μ^{int} , $\tilde{V}_\mu^{\text{int}}$) with diagonal kinetic terms. The second rotation, after EW symmetry breaking

⁴ The other possibility, i.e., the dark sector has direct couplings with the SM fermions is reviewed recently in ref. [34].

(EWSB), via angle $\theta_{\widetilde{W}}$, takes this B_μ^{int} together with W_μ^3 to the intermediate $A_\mu, Z_\mu^{\text{int}}$ basis. Finally, the third rotation through another angle ϕ , leaving the massless photon aside, takes $Z_\mu^{\text{int}}, \widetilde{V}_\mu^{\text{int}}$ to the Z_μ, Z'_μ basis where Z_μ, Z'_μ are associated with the physical Z and Z' boson. In summary, the initial $B_\mu, W_\mu^3, \widetilde{V}_\mu$ basis can be related to the physical A_μ, Z_μ, Z'_μ basis in the following way:

$$\begin{pmatrix} B_\mu \\ W_{3\mu} \\ \widetilde{V}_\mu \end{pmatrix} = \begin{pmatrix} c_{\widetilde{W}} & -s_{\widetilde{W}}c_\phi + t_\delta s_\phi & -s_{\widetilde{W}}s_\phi - t_\delta c_\phi \\ s_{\widetilde{W}} & c_{\widetilde{W}}c_\phi & c_{\widetilde{W}}s_\phi \\ 0 & -\frac{s_\phi}{c_\delta} & \frac{c_\phi}{c_\delta} \end{pmatrix} \begin{pmatrix} A_\mu \\ Z_\mu \\ Z'_\mu \end{pmatrix}, \quad (2)$$

where $t_\delta, c_\delta, c_{\widetilde{W}}, s_{\widetilde{W}}, s_\phi, c_\phi \equiv \tan \delta, \cos \delta, \cos \theta_{\widetilde{W}}, \sin \theta_{\widetilde{W}}, \sin \phi, \cos \phi$ with:

$$\tan 2\phi = \frac{\widetilde{m}_Z^2 s_{\widetilde{W}} \sin 2\delta}{m_V^2 - \widetilde{m}_Z^2 (c_\delta^2 - s_{\widetilde{W}}^2 s_\delta^2)}, \quad (3)$$

here $s_\delta \equiv \sin \delta$. The quantities $\theta_{\widetilde{W}}, \widetilde{m}_Z$ do not represent the measured values of Weinberg angle and Z -boson mass [78] but are related to them as will be explained later. The masses of Z' and Z are written as:

$$m_{Z',Z}^2 = \frac{1}{2} \left[\widetilde{m}_Z^2 (1 + s_{\widetilde{W}}^2 t_\delta^2) + \frac{m_V^2}{c_\delta^2} \pm \sqrt{(\widetilde{m}_Z^2 (1 + s_{\widetilde{W}}^2 t_\delta^2) + \frac{m_V^2}{c_\delta^2})^2 - \frac{4}{c_\delta^2} \widetilde{m}_Z^2 m_V^2} \right], \quad (4)$$

which gives $m_Z \simeq \widetilde{m}_Z$ in the experimentally favoured limit $\delta \ll 1$, along with $m_{Z'} \simeq m_V$.

Notice that the transformation used in eq. (2) is valid only if one of these two conditions is met:

$$\begin{aligned} \frac{m_V^2}{\widetilde{m}_Z^2} &\geq 1 + 2s_{\widetilde{W}} \tan^2 \delta + 2\sqrt{s_{\widetilde{W}}^2 \tan^2 \delta (1 + s_{\widetilde{W}}^2 \tan^2 \delta)}, \\ \frac{m_V^2}{\widetilde{m}_Z^2} &\leq 1 + 2s_{\widetilde{W}} \tan^2 \delta - 2\sqrt{s_{\widetilde{W}}^2 \tan^2 \delta (1 + s_{\widetilde{W}}^2 \tan^2 \delta)}. \end{aligned} \quad (5)$$

One should note that the transformation of eq. (2) does not change the photon coupling [74], implying the following identity:

$$s_{\widetilde{W}} c_{\widetilde{W}} \widetilde{m}_Z^2 = s_W c_W m_Z^2 = \frac{\pi \alpha(m_Z)}{\sqrt{2} G_F}, \quad (6)$$

where $s_W, c_W \equiv \sin \theta_W, \cos \theta_W$ are associated with the measured value of Weinberg angle θ_W [78]. $\alpha(m_Z)$ is the fine structure constant at the energy scale m_Z and G_F represents the Fermi constant [78].

One should also consider the invariance of W -boson mass under the transformation of eq. (2), i.e., $m_W^2 = m_Z^2 c_W^2 = \widetilde{m}_Z^2 c_{\widetilde{W}}^2$ which allows us to express the ρ parameter [78] as:

$$\rho = \frac{\widetilde{m}_Z^2 c_{\widetilde{W}}^2}{m_Z^2 c_W^2}, \quad (7)$$

with the experimental measured value given by $\rho - 1 = 4_{-4}^{+8} \times 10^{-4}$ [78]. Further, from the EWPT one can consider a simple and conservative limit on δ as [75, 79]:

$$\delta \lesssim \arctan \left[0.4 \left(\frac{m_{Z'}}{\text{TeV}} \right) \right]. \quad (8)$$

It is now apparent that one can use eq. (6), eq. (7) and eq. (8) to discard experimentally disfavoured values of the kinetic mixing parameter δ . Further constraints on δ can emerge from various other experimental observations. The mixing among B_μ , W_μ^3 and \tilde{V}_μ (see eq. (2)), couples the SM fermions and the DM with the Z boson. The latter coupling implies an enhancement of the invisible Z decay width for $2m_X < m_Z$. Hence, the parameter δ , along with m_V , will receive constraints from a plethora of different collider searches like dileptons ($pp \rightarrow Z' \rightarrow e^+e^-, \mu^+\mu^-$) [80–82], dijets ($pp \rightarrow Z' \rightarrow q\bar{q}$) [83–86], mono- \mathbf{X} ($pp \rightarrow Z' + \mathbf{X}$, $Z' \rightarrow \text{DM pairs}$) with $\mathbf{X} = q/g$ [87], W [88], Z [88, 89], γ [90–92], SM-Higgs [93–95], etc., invisible Z decay width [78] and a few others. The dijets and mono- \mathbf{X} searches also restrict the parameters α_{CS} , m_X . Finally, the DM phenomenology, i.e., the correct relic density, DD and ID results will also put limits on the parameters δ , α_{CS} , m_V and m_X . We note in passing that for numerical analyses we have traded the parameter m_V with the physical mass $m_{Z'}$ using eq. (4).

In the mass basis, the Lagrangian relevant for our subsequent analysis is given by:

$$\begin{aligned} \mathcal{L}_{Z/Z', SM} = & \bar{f}\gamma^\mu (g_{f_L}^Z P_L + g_{f_R}^Z P_R) f Z_\mu + \bar{f}\gamma^\mu (g_{f_L}^{Z'} P_L + g_{f_R}^{Z'} P_R) f Z'_\mu \\ & + g_W^Z [[W^+ W^- Z]] + g_W^{Z'} [[W^+ W^- Z']] + \frac{g_{hZZ}}{2} Z^\mu Z_\mu h + g_{hZZ'} Z'_\mu Z^\mu h + \frac{g_{hZ'Z'}}{2} Z'_\mu Z'^\mu h \\ & - \alpha_{\text{CS}} \frac{s_\phi}{c_\delta} \epsilon^{\mu\nu\rho\sigma} X_\mu X_{\rho\sigma} Z_\nu + \alpha_{\text{CS}} \frac{c_\phi}{c_\delta} \epsilon^{\mu\nu\rho\sigma} X_\mu X_{\rho\sigma} Z'_\nu, \end{aligned} \quad (9)$$

here $P_{L(R)} = (1 \pm \gamma_5)/2$ and

$$\begin{aligned} g_{f_L}^Z &= g_Y Y_L (-s_W c_\phi + t_\delta s_\phi) + g_W I_z (c_W c_\phi), & g_{f_R}^Z &= g_Y Y_R (-s_W c_\phi + t_\delta s_\phi), \\ g_{f_L}^{Z'} &= g_Y Y_L (-s_W s_\phi - t_\delta c_\phi) + g_W I_z (c_W s_\phi), & g_{f_R}^{Z'} &= g_Y Y_R (-s_W s_\phi - t_\delta c_\phi), \end{aligned} \quad (10)$$

where g_Y is the gauge coupling of $U(1)_Y$, I_z is the 3rd component of the weak isospin, $Y_{L,R}$ are hypercharge of the left- and right- chiral fermions, g_W is the $SU(2)_L$ gauge coupling.

$$g_W^Z = g_W c_W c_\phi, \quad g_W^{Z'} = g_W c_W s_\phi, \quad (11)$$

$$\begin{aligned} g_{hZZ} &= 2v_h \left[\frac{g_Y}{2} (-s_W c_\phi + t_\delta s_\phi) - \frac{g_W}{2} (c_W c_\phi) \right]^2, \\ g_{hZZ'} &= 2v_h \left[\frac{g_Y}{2} (-s_W s_\phi - t_\delta c_\phi) - \frac{g_W}{2} (c_W s_\phi) \right] \left[\frac{g_Y}{2} (-s_W c_\phi + t_\delta s_\phi) - \frac{g_W}{2} (c_W c_\phi) \right], \\ g_{hZ'Z'} &= 2v_h \left[\frac{g_Y}{2} (-s_W s_\phi - t_\delta c_\phi) - \frac{g_W}{2} (c_W s_\phi) \right]^2, \end{aligned} \quad (12)$$

here v_h is the vacuum expectation value (VEV) of the SM-Higgs doublet and a factor ‘2’ appears in ZZh , $Z'Z'h$ vertices due to the presence of identical particles. For the $\alpha_{\text{CS}} \frac{-s_\phi(c_\phi)}{c_\delta} \epsilon^{\mu\nu\rho\sigma} X_\mu X_{\rho\sigma} Z_\nu(Z'_\nu)$ term, considering the following momentum assignments $X_\mu(p_a)X_\nu(p_b)Z_\rho/Z'_\rho$ one can use

$$g_X^Z = -2\alpha_{\text{CS}} \frac{s_\phi}{c_\delta}, \quad g_X^{Z'} = 2\alpha_{\text{CS}} \frac{c_\phi}{c_\delta}, \quad (13)$$

for subsequent relevant analytical formulae like DM pair annihilation cross-section etc. Once again the factor ‘2’ appears due to identical particles. Lastly

$$[[W^+W^-Z(Z')]] \equiv i \left[W_{\mu\nu}^+ W^{-\mu} Z(Z')^\nu - W_{\mu\nu}^- W^{-\mu} Z(Z')^\nu + \frac{1}{2} Z(Z')^{\mu\nu} (W_\mu^+ W_\nu^- - W_\nu^+ W_\mu^-) \right]. \quad (14)$$

With these analytical expressions now we will discuss the DM phenomenology of this framework in the next subsection.

A. Dark Matter Phenomenology

In this subsection we discuss the DM phenomenology in the light of various constraints coming from the requirement of correct relic density and consistency with the existing and/or upcoming DD and ID results. The DM is produced in the early Universe according to the WIMP paradigm. We will subsequently discuss how these observations can affect the accessibility of the chosen set-up at the present or in the near future DM detection experiments, assuming projected search sensitivities. Nevertheless, for the sake of completeness, we will also qualitatively discuss the complementary limits arising from the EWPT, collider searches, etc. We start our discussion in the context of accommodating correct relic density and successively will address the restrictions coming from direct and indirect DM searches.

1. Relic density

It is well known that according to the WIMP paradigm a single particle species can account for the correct DM relic density $\Omega_X h^2 \propto 1/\langle\sigma v\rangle$, where $\langle\sigma v\rangle$ represents the thermally averaged DM pair annihilation cross-section into the SM states. The experimentally hinted value $\Omega_X h^2 \approx 0.12$ [6] predicts $\langle\sigma v\rangle, \sim \mathcal{O}(10^{-26} \text{ cm}^3 \text{ s}^{-1})$.

In the chosen framework (see Section II), the DM pair can annihilate into the SM fermions ($\bar{f}f$) and W^+W^- , as well as in Zh and $Z'h$ final states, through s-channel exchange of the Z/Z' boson, and into ZZ , ZZ' and $Z'Z'$ final states, through t-channel exchange of a DM state. Approximate

analytical expressions of the corresponding annihilation cross-sections are obtained through the expansion $\langle\sigma v\rangle \simeq a + b\frac{1}{x} + \dots$ with $x = \frac{m_X}{T}$ [96, 97], T being the temperature. We remind, however, that the aforesaid approximation is not reliable over the entire parameter space [98], e.g., the pole regions $m_X \sim \frac{m_{Z,Z'}}{2}$. Hence, all results presented in this article are obtained through full numerical computations using the package micrOMEGAs [99–101], after implementing the model in FeynRules [102, 103]. The DM annihilation cross-sections in the possible final states are given as:

- $XX \rightarrow \bar{f}f$:

$$\begin{aligned} \langle\sigma v\rangle_{\bar{f}f} \simeq & \frac{n_c m_f^2}{3\pi} \sqrt{1 - \frac{m_f^2}{m_X^2}} \left(\frac{(g_{f_L}^Z - g_{f_R}^Z) g_X^Z}{m_Z^2} + \frac{(g_{f_L}^{Z'} - g_{f_R}^{Z'}) g_X^{Z'}}{m_{Z'}^2} \right)^2 \frac{1}{x} \\ & + \frac{n_c}{108\pi} \left(\frac{(g_X^Z)^2 \left((g_{f_L}^Z)^2 + (g_{f_R}^Z)^2 \right)}{m_Z^4} + \frac{(g_X^{Z'})^2 \left((g_{f_L}^{Z'})^2 + (g_{f_R}^{Z'})^2 \right)}{m_{Z'}^4} \right. \\ & \left. + \frac{2g_X^{Z'} g_X^Z \left(g_{f_L}^{Z'} g_{f_L}^Z + g_{f_R}^{Z'} g_{f_R}^Z \right)}{m_{Z'}^2 m_Z^2} \right) \frac{1}{x^2}, \end{aligned} \quad (15)$$

where we have written not only the leading $1/x$ (p-wave) term but also the second order $1/x^2$ (d-wave) one which appears to be the dominant one since the first one is suppressed by the square of SM fermion mass m_f^2 . The parameter n_c denotes colour factor with a value of 3 (1) for quarks (leptons).

- $XX \rightarrow W^+W^-$:

$$\langle\sigma v\rangle_{W^+W^-} \simeq \frac{5}{9\pi m_W^4} \left(\frac{g_X^Z g_W^Z m_X}{4} - \frac{g_X^{Z'} g_W^{Z'} m_X^3}{m_{Z'}^2} \right)^2 \frac{1}{x^2}, \quad \text{for } m_{W,Z} \ll m_X \ll m_{Z'}. \quad (16)$$

- $XX \rightarrow Zh$:

$$\langle\sigma v\rangle_{Zh} \simeq \frac{2}{3\pi} \frac{m_X^6}{m_Z^6} \left(\frac{g_X^Z g_{hZZ}}{4m_X^2} - \frac{g_X^{Z'} g_{hZZ'}}{m_{Z'}^2} \right)^2 \frac{1}{x}, \quad \text{for } m_Z \sim m_h \ll m_X \ll m_{Z'}. \quad (17)$$

- $XX \rightarrow Z'h$:

$$\langle\sigma v\rangle_{Z'h} \simeq \frac{1}{24\pi} \frac{m_X^2}{m_{Z'}^6} \left(g_{hZZ'} g_X^Z + g_{hZ'Z'} g_X^{Z'} \right)^2 \frac{1}{x}, \quad \text{for } m_Z \sim m_h \ll m_{Z'} \ll m_X. \quad (18)$$

- $XX \rightarrow ZZ$:

$$\langle\sigma v\rangle_{ZZ} \simeq \frac{8\alpha_{\text{CS}}^4 \delta^4 m_X^2 m_Z^4 s_W^4}{9\pi m_{Z'}^8}, \quad \text{for } m_Z \ll m_X \ll m_{Z'}. \quad (19)$$

- $XX \rightarrow Z'Z'$:

$$\langle\sigma v\rangle_{Z'Z'} \simeq \frac{8\alpha_{\text{CS}}^4 m_X^2}{9\pi m_{Z'}^4}, \quad \text{for } m_Z \ll m_{Z'} \ll m_X. \quad (20)$$

- $XX \rightarrow Z'Z$:

$$\langle\sigma v\rangle_{Z'Z} \simeq \frac{16\alpha_{\text{CS}}^4 \delta^2 m_X^2 m_Z^2 s_W^2}{9\pi m_{Z'}^6}, \quad \text{for } m_Z \ll m_{Z'} \ll m_X. \quad (21)$$

As evident from the above expressions that annihilation channels originated by s-channel exchange of the Z/Z' feature a suppressed annihilation cross-section, at least p-wave or even d-wave in the cases of W^+W^- and $\bar{f}f$ final states (see eq. (16) and eq. (15)). For the latter a p-wave contribution is also present but it is helicity suppressed. The t-channel induced annihilations feature, instead, a s-wave cross-section. The cross-section into ZZ pairs (see eq. (19)) is anyway suppressed by an higher power of the kinetic mixing parameter δ , with respect to the other annihilation channels.

The DM pair annihilation cross-section, as depicted in figure 1, typically lies much below the thermally favored value, i.e., $10^{-26} \text{ cm}^3 \text{ s}^{-1}$, ad exception of the pole regions $m_X \sim m_Z/2, m_{Z'}/2$, or DM masses above several hundreds of GeV so that at least annihilations into ZZ' final state appears kinematically accessible.

2. Indirect Detection

Residual annihilation processes of the DM at the present times could be efficient enough so that they might be detected by the Earth based telescopes or satellites. The absence of definite signals till date are translated into upper bounds on $\langle\sigma v\rangle$ as a function of the DM mass. At the moment, the strongest limits come from searches of the gamma-rays produced in the DM annihilations. For DM masses below a few hundred GeVs, these limits are set by the FERMI satellite [104] and exclude the thermally favored values of $\langle\sigma v\rangle$ for $m_X < 100$ GeV. For higher values of m_X the best sensitivity is achieved by HESS [105] which has put a limit $\langle\sigma v\rangle \lesssim 10^{-25} \text{ cm}^3 \text{ s}^{-1}$ for $m_X \sim 1$ TeV, considering a Einasto density profile for the DM.

As shown earlier while discussing the relic density that most of the DM annihilation processes have a p-wave (or even d-wave) annihilation cross-section, i.e., they are velocity dependent. As a consequence the DM annihilation at present times is suppressed by several orders of magnitude with respect to its value at the thermal freeze-out and thus, limits from DM ID are actually not effective. ID can probe the WIMP paradigm for the DM relic density only when the latter is mostly

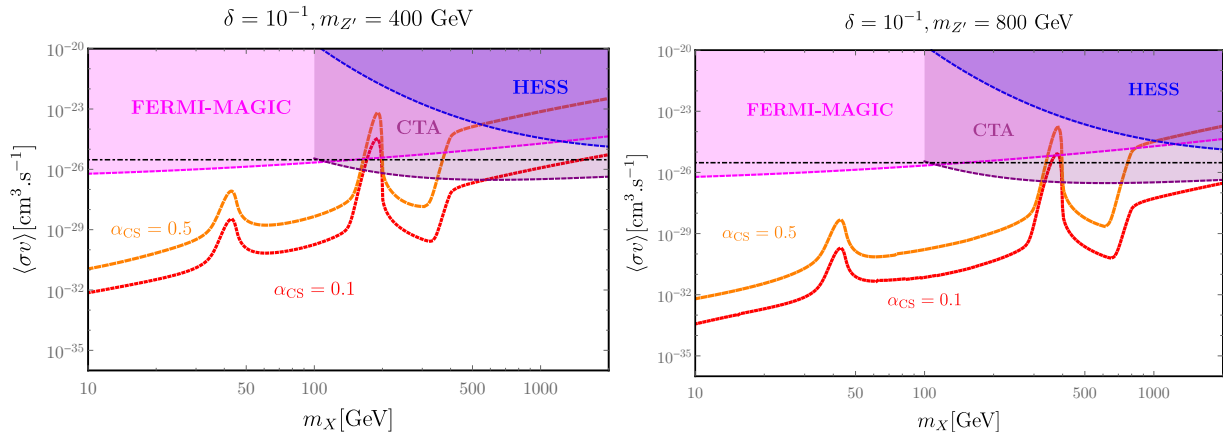


Figure 1. Variation of the thermally averaged DM pair annihilation cross-section $\langle\sigma v\rangle$, at thermal freeze-out, as function of the DM mass m_X for $m_{Z'} = 400$ GeV (left) and 800 GeV (right) with two values of $\alpha_{CS} = 0.1$ (red coloured solid line) and 0.5 (orange coloured solid line) keeping kinetic mixing parameter $\delta = 0.1$. The black coloured dashed line represents the thermally favored value of $\langle\sigma v\rangle = 3 \times 10^{-26} \text{ cm}^3 \text{ s}^{-1}$. The magenta coloured region with dashed outline represents the resultant exclusion from the combined FERMI-LAT and MAGIC observations (abbreviated as FERMI-MAGIC in all the successive relevant figures) while the blue coloured region with dashed boundary represents the region already excluded by HESS for a Einasto density profile of the DM. Finally, the purple colour region with dashed outline represents the expected future exclusion from CTA.

determined by processes with an s-wave (i.e., velocity independent) annihilation cross-section. In our setup this requirement is fulfilled by annihilation into $Z'Z$ and $Z'Z'$ states (see eq. (21) and eq. (20)). The other s-wave dominated annihilation into ZZ final state (see eq. (19)), as already addressed, is insignificant as it is suppressed by the fourth power of kinetic mixing parameter δ .

We have thus compared the DM annihilation cross-section into $Z'Z$ and $Z'Z'$ final states with the limits derived from combined analysis of the MAGIC and FERMI-LAT observations (abbreviated as FERMI-MAGIC) of the dwarf spheroidal galaxies (dSphs) [106]. We also consider limits from 10 years of observations towards the inner galactic halo by HESS [107]. In the absence of a dedicated analysis for the considered final states we have applied the limit for gamma-rays originating from W^+W^- pairs. This choice is reasonable since the Z' decays efficiently into hadrons as the SM gauge bosons. Any mild change in the limits as a result of this assumption is beyond the scope of our current work.

Our results are reported in figure 1 concerning changes of the DM pair annihilation cross-section at thermal freeze-out with the DM mass m_X , for specific assignments of the other relevant inputs, detailed in the figure caption. As evident from this figure that the impact of ID limits from FERMI-

MAGIC (magenta coloured region) and HESS (blue coloured region) appears to be rather limited. This can be understood by looking at this simple analytical estimate for $\langle\sigma v\rangle_{Z'Z'}$:

$$\langle\sigma v\rangle_{Z'Z'} \simeq \frac{8\alpha_{\text{CS}}^4 m_X^2}{9\pi m_{Z'}^4} \simeq 3 \times 10^{-28} \text{cm}^3 \text{s}^{-1} \left(\frac{\alpha_{\text{CS}}}{0.1}\right)^4 \left(\frac{m_X}{1 \text{ TeV}}\right)^2 \left(\frac{m_{Z'}}{1 \text{ TeV}}\right)^{-4}, \quad (22)$$

which shows that a value of the cross-section equal or bigger than the thermal expectation i.e., $\sim \mathcal{O}(10^{-26} \text{cm}^3 \text{s}^{-1})$, can be achieved only for masses of the Z' not exceeding a few hundreds of GeV and/or $\alpha_{\text{CS}} \sim 0.5$. Such value of α_{CS} , however, is somewhat extreme since this coupling is expected to have a radiative origin as will be discussed later. The impact of possible limits from ID will be anyway increased in the near future by Cherenkov Telescope Array a.k.a. CTA [108–113] which we have reported (purple coloured region) in figure 1, assuming a projected limits from 500 h of observation towards the galactic center.

3. Direct detection

DD experiments aim at measuring the recoil energy released by an atomic nuclei upon a scattering process with a DM state. Several experiments have performed searches for DM scattering off nuclei reaching, in the last year, an impressive sensitivity. In particular, in the case of Spin Independent (SI) interactions of the DM with nuclei, a cross-section $\sim \mathcal{O}(10^{-46} \text{cm}^2)$, for DM mass of 50 GeV, has been excluded by the LUX [114] and PandaX [115]. These experiments play also a leading role in constraining the Spin Dependent (SD) interactions. In this case the maximal sensitivity is achieved for DM mass of 40 GeV which corresponds to a value $\sim 10^{-41} \text{cm}^2$ of the DM-nucleon scattering cross-section [116].

In the chosen setup (see eq. (1)), scattering of the DM with nucleons is originated, at the microscopic level, by an interaction between the DM and the SM quarks mediated via t-channel exchange of the Z/Z' boson. An interaction of this kind, in the non-relativistic limit, is described by the following effective operator [100]:

$$\mathcal{L}_{\text{DM scattering}} = \left(\frac{g_X^Z a_q^Z}{m_Z^2} + \frac{g_X^{Z'} a_q^{Z'}}{m_{Z'}^2} \right) (\partial_\alpha X_\beta X_\nu - X_\beta \partial_\alpha X_\nu) \epsilon^{\alpha\beta\nu\mu} \bar{q} \gamma_\mu \gamma_5 q, \quad (23)$$

where $a_q^{Z'} = \frac{g_{qR}^{Z'} - g_{qL}^{Z'}}{2}$ and $a_q^Z = \frac{g_{qR}^Z - g_{qL}^Z}{2}$, which corresponds to a SD interaction with squared amplitude:

$$|\overline{\mathcal{M}}|^2 = \frac{32m_X^2 m_N^2}{m_Z^4 m_{Z'}^4} \left(\sum_q a_q^Z \Delta_q^N g_X^Z m_{Z'}^2 + \sum_q a_q^{Z'} \Delta_q^N g_X^{Z'} m_Z^2 \right)^2, \quad (24)$$

with m_N denoting the mass of a nucleon $N = p, n$ while Δ_q^N represents the contribution of the quark q to the spin of the nucleon N . The SD scattering cross-section can be straightforwardly derived, taking into account the multiple isotopes present in the detector material as:

$$\sigma_{Xp}^{\text{SD}} = \frac{2}{\pi} \frac{\mu_{Xp}^2}{m_Z^4 m_{Z'}^4} \frac{\sum_A \eta_A \left(S_Z^A g_X^Z m_{Z'}^2 + S_{Z'}^A g_X^{Z'} m_Z^2 \right)^2}{\sum_A \eta_A \left(S_n^A + S_p^A \right)^2}, \quad (25)$$

where $\mu_{Xp} = m_X m_p / (m_X + m_p)$ is the reduced mass for the DM-proton system and $S_{Z^{(\prime)}}^A = a_u^{Z^{(\prime)}} (\Delta_u^p S_p^A + \Delta_d^p S_n^A) + a_d^{Z^{(\prime)}} [(\Delta_d^p + \Delta_s^p) S_p^A + (\Delta_u^p + \Delta_s^p) S_n^A]$. Here $S_{p,n}^A$ represents the contribution of protons and neutrons to the spin of a nucleus with atomic number A while η_A represents the relative abundance of a given isotope of the element constituting the target material. Notice that the result is almost independent of the DM mass since the only dependence through μ_{Xp} will vanish for $m_X \gg m_p$ giving $\mu_{Xp} \sim m_p$. A simple estimate of σ_{Xp}^{SD} can be performed assuming $\delta, \alpha_{\text{CS}} \ll 1$ as:

$$\sigma_{Xp}^{\text{SD}} \simeq 6 \times 10^{-50} \text{cm}^2 \left(\frac{\delta}{0.1} \right)^2 \left(\frac{\alpha_{\text{CS}}}{0.1} \right)^2 \left(\frac{m_{Z'}}{1 \text{ TeV}} \right)^{-4}, \quad (26)$$

which gives values of σ_{Xp}^{SD} well below the current maximal sensitivity (10^{-41}cm^2), and remains also beyond the reach of next generation detectors for the chosen set of parameter values, consistent with other existing constraints.

B. Collider phenomenology

Phenomenological models, where the DM candidate interacts with the SM fields through a spin-1 mediator typically possess a rich collider phenomenology. In the case when on-shell production of a Z' is kinematically accessible in proton-proton collision, detectable signals can appear from the decays of Z' into SM fermions, showing a new resonance in the invariant mass distribution of dijets [83–86] or dileptons [80–82] as well as from possible decay of a Z' into DM pairs which can be probed through mono- \mathbf{X} searches (\mathbf{X} = hadronic jets, photon, weak gauge bosons, SM-Higgs) [87–95] accompanied by moderate/large missing transverse energy/momentum. Interestingly, the relative relevance of these two kinds of searches, i.e., resonances and mono- \mathbf{X} events, is mainly set by the invisible decay branching fraction (Br) of the Z' which, in turn, is constrained by the DM observables that primarily appears from the requirement of correct relic density for the chosen framework.

The impact of experimental limits from resonance searches is depicted in figure 2 where, for simplicity, we consider $2m_X > m_{Z'}$ to forbid $Z' \rightarrow \text{DM pairs}$ process. For these analyses we consider all possible quark flavours including top for $m_{Z'} > 2m_t$ regime while $l = e$ and μ only. Here

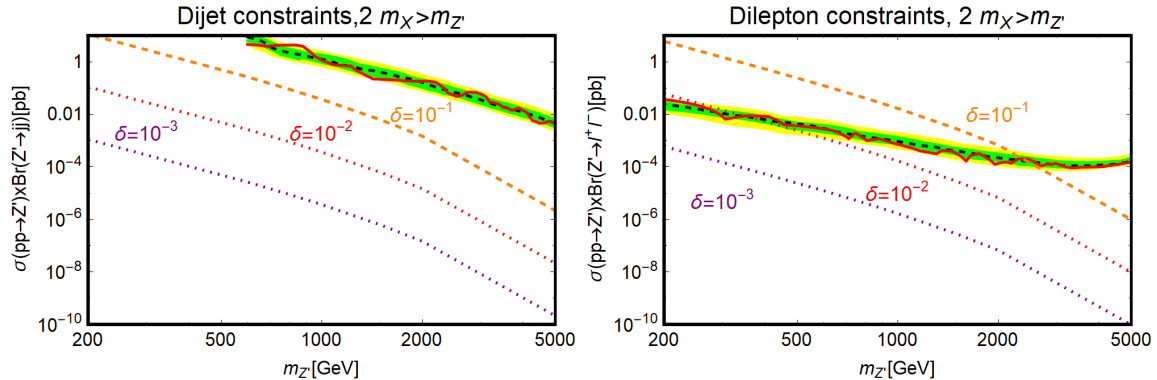


Figure 2. Comparison of the production cross-sections for $pp \rightarrow Z' \rightarrow jj$ (left panel) and $pp \rightarrow Z' \rightarrow l^+l^-$ (right panel) processes for an on-shell Z' in the chosen theory framework with the relevant experimental limits [83] and [82], respectively, as a function of $m_{Z'}$ for three fixed values of $\delta = 10^{-3}$, 10^{-2} and 10^{-1} . Here the solid red coloured curve represents the observed experimental limit while dashed black coloured line, green and yellow coloured bands represent the expected limit and its 1σ , 2σ ranges. The dotted purple, red and dashed orange coloured lines are used for $\delta = 0.001$, 0.01 and 0.1 configurations, respectively. For simplicity, we have considered the case of $2m_X > m_{Z'}$ so that Z' has only visible decays. In our analysis we consider $j = u, d, c, s, b$ and t for $m_{Z'} > 2m_t$ and $l = e, \mu$.

we have compared the results of numerical simulations for the chosen setup with the experimental ones including 1σ , 2σ variations of the production cross-sections as observed in refs. [83] and [82], respectively. Since the Z' -SM fermions mixing (see eq. (10)) appears from an effective Z - Z' mixing, both $\sigma(pp \rightarrow Z')$ and $\text{Br}(Z \rightarrow jj/l^+l^-)$ are sensitive to the parameter δ . The resultant δ^2 dependence thus, hints diminishing $\sigma(pp \rightarrow Z') \times \text{Br}(Z' \rightarrow jj/l^+l^-)$ values for decreasing δ values, as also reflected in figure 2. It is evident from figure 2 that once values of the kinetic mixing parameter δ smaller than $\mathcal{O}(1)$ are considered to comply with the theoretical and EWPT (see eq. (8)) constraints, only the limits from dileptons resonance searches remain effective. For $\delta = 0.1$, values of $m_{Z'}$ below 2 TeV are ruled out while for $\delta = 0.01$, a much weaker lower bound of approximately 300 GeV is obtained on $m_{Z'}$. For further lower values of δ , very small δ^2 dependence⁵ makes $m_{Z'}$ unconstrained from the aforesaid searches.

In the presence of a non-zero and sizable invisible branching fraction for Z' , i.e., $\text{Br}(Z' \rightarrow \text{DM pairs})$, the production cross-sections of dijets/dileptons get suppressed by the enhanced decay width of Z' . In such a scenario, the cross-section corresponding to mono- \mathbf{X} signals might become sizable, possibly providing complementary constraints. We preserve the discussion of such complementary signals for the next subsection.

⁵ Holds true for a resonant production with no/suppressed invisible decay of Z' .

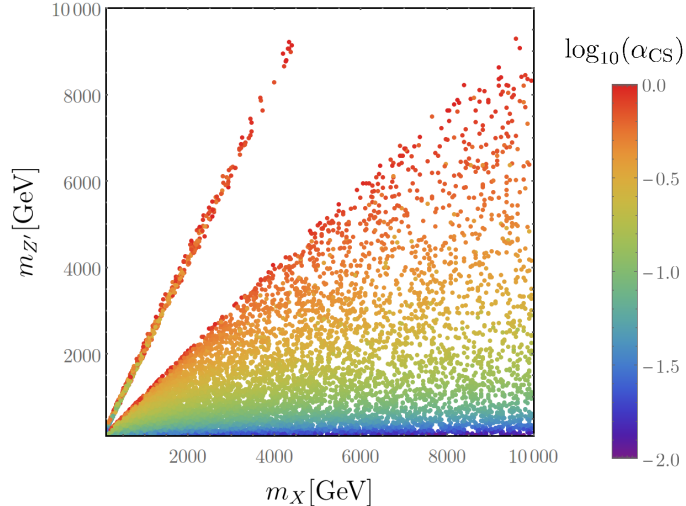


Figure 3. Summary of results in the bi-dimensional plane $m_X, m_{Z'}$ for a vectorial DM with Z' -portal in the presence of CS interaction and kinetic mixing terms. The colour code corresponds to the variation in α_{CS} values. The plot reports model points, generated through a parameter scan, illustrated in the main text, passing constraints from the DM phenomenology and general constraints on the kinetic mixing parameter.

C. Results

In this subsection we report the impact of various constraints, as mentioned in the previous subsections, on the parameter space of the model. As already pointed out the effect of DD and ID constraints on our model framework is substantially negligible. Concerning the DM phenomenology, the only relevant constraint comes from the requirement of the correct relic density. We have then conducted a more extensive analysis, with respect to the one presented in figure 1 by performing a scan over the four free input parameters in the following ranges:

$$\delta \in [10^{-3}, 1], \quad \alpha_{CS} \in [10^{-2}, 1], \quad m_X \in [100 \text{ GeV}, 10 \text{ TeV}], \quad m_{Z'} \in [100 \text{ GeV}, 10 \text{ TeV}], \quad (27)$$

and retaining the model points featuring the correct DM relic density⁶ and respecting, at the same time, constraints from the EWPT, SM ρ -parameter measurement as well as reproducing experimentally viable mass and width for the Z -boson. The ensemble of points respecting these aforementioned constraints has been reported in figure 3, in the m_X - $m_{Z'}$ bi-dimensional plane with a colour code showing variations in α_{CS} values.

As evident from figure 3, in agreement with the general discussion of sub-subsection II A 1, that the correct relic density can be achieved either in the “pole” region $m_X \sim \frac{m_{Z'}}{2}$ or for $m_X \gtrsim m_{Z'}$,

⁶ We consider points corresponding to $\Omega_X h^2 = 0.12 \pm 10\%$ variation.

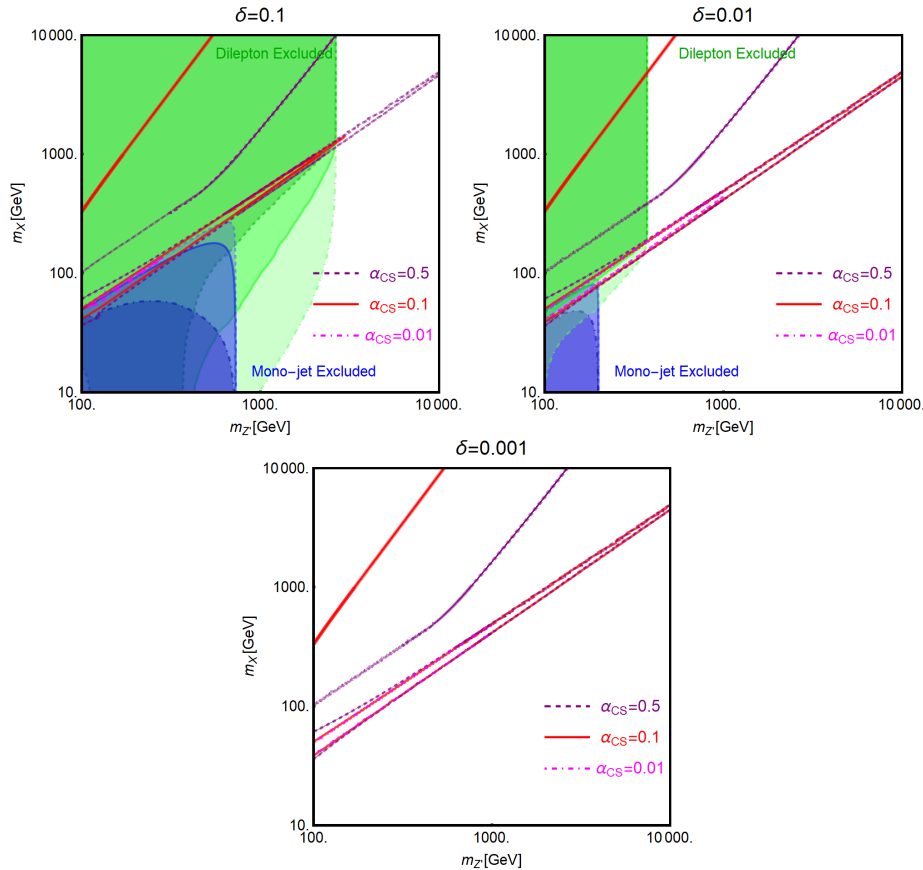


Figure 4. Summary of the relic density and the collider constraints in the $(m_{Z'}, m_X)$ bi-dimensional plane for the three values of δ , 0.1 (top-left), 0.01 (top-right) and 0.001 (bottom) choosing three assignments of α_{CS} , namely 0.5, 0.1, and 0.01. In each plots the dashed magenta, solid red and dot-dashed purple coloured curves represent the correct DM relic density for $\alpha_{CS} = 0.5, 0.1$ and 0.01 , respectively. The regions covered by the light blue colour with dashed boundary, blue colour with solid outline and dark blue colour with dot-dashed boundary are excluded by mono-jet searches when one considers the value of $\alpha_{CS} = 0.5, 0.1$ and 0.01 , respectively. The same set of α_{CS} values is associated with the three different regions, namely, dark green coloured with dashed boundary, green coloured with solid outline and light green coloured with dot-dashed boundary, respectively, that are excluded from the searches of dilepton resonances.

when the process $XX \rightarrow Z'Z'$ is kinematically allowed⁷. We have successively examined the impact of collider constraints on our construction in figure 4. For a better and elucidate illustration of our findings, we have considered three fixed assignments of δ , namely 0.001, 0.01 and 0.1 and

⁷ As can be noticed from the analytical expression (see eq. (20)) that the annihilation cross-section into $Z'Z'$ increases with the DM mass. This is somewhat an unreasonable behavior possibly leading to the violation of unitarity (see, for example, refs. [37, 38, 51, 117, 118]). We emphasize here that the studied phenomenological Lagrangian is actually the low-energy effective theory limit of a more complete framework. Thus, violation of unitarity for some assignments of the model parameters would simply imply that for those parameter values the effective field theory limit is invalid and hence, additional degrees of freedom should be included to develop a UV complete theory. We have verified that possible consequence of the unitarity violation would affect the thermal DM region only when $\alpha_{CS} \gtrsim \mathcal{O}(1)$. The results of our findings as reported in figure 4 are instead not affected by this limit as we have considered lower values of α_{CS} parameter.

the same for α_{CS} , 0.01, 0.1 and 0.5 keeping m_X and $m_{Z'}$ as the two free varying input parameters. The relevant results are reported in the three panels of figure 4 corresponding to the three different values of δ , namely 0.1 (top-left), 0.01 (top-right) and 0.001 (bottom) where isocontours of the correct DM relic density are shown for the three assignments of α_{CS} parameter using three different representations (purple coloured dot-dashed line for $\alpha_{CS} = 0.01$, solid red coloured line for $\alpha_{CS} = 0.1$ and magenta coloured dashed line for $\alpha_{CS} = 0.5$). These isocontours have been compared with the limits from dilepton resonances and mono-jet searches. The former is evaluated in a similar fashion as of figure 2 by computing the associated cross-section, as a function of the input parameters δ, α_{CS}, m_X and $m_{Z'}$ using the package MadGraph5_aMC@NLO [119] and compared with the relevant experimental observations. Contrary to what we did earlier, now we have also accounted for the possibility of a sizable invisible branching fraction of Z' by suitably rescaling the experimental limit according to the procedure illustrated in ref. [54]. As evidenced from the top-left panel of figure 4 that the previously quoted limit of approximately 2 TeV (see figure 2, right panel plot) for $\delta = 0.1$ is actually effective only when $m_{Z'} < 2m_X$. When decay of a Z' into DM pairs is kinematically accessible, i.e., $m_{Z'} > 2m_X$, and $\alpha_{CS} \gtrsim \mathcal{O}(1)$, the lower limit on $m_{Z'}$ can be reduced even to a few hundreds of GeV. The mono-jet limits have been derived by evaluating the production cross-section times the detector efficiency and acceptance in the selection of the final state by generating and analyzing events, corresponding to the process $pp \rightarrow XXj$, through the combination of MadGraph5_aMC@NLO [119] (matrix element calculation) PYTHIA 8 [120] (event generation and hadronization) and DELPHES 3 (fast detector simulations) [121]. The selection acceptance for the generated events has been determined by imposing a minimal value of 500 GeV for the missing transverse energy. The mono-jet limits have been determined by imposing an upper bound of ~ 6 fb on the product of production cross-section, signal acceptance and the detection efficiency [85]. Our procedure has been validated by reproducing the excluded region for the benchmark model adopted in ref. [85].

It is apparent from figure 4 that both kinds of the collider limits, i.e., dileptons and mono-jet, are essentially effective for large and moderate values of δ , i.e., significant for $\delta = 0.1$ (top-left panel) and moderate for $\delta = 0.01$ (top-right panel). These behaviours, as already stated, are expected since the parameter δ determines the production vertex of a Z' as well as its decay rate into the SM fermions. Hence, collider production cross-section suppresses very fast as the kinetic mixing parameter decreases. On the contrary, the requirement of the correct relic density is more moderately affected by the decrease in the value of the kinetic mixing parameter. This happens because the correct relic density is achieved mostly through the annihilation into $Z'Z'$ final states,

whose rate does not depend on δ , or in the ‘‘pole’’ region, where variations of the couplings can be compensated by slight changes of $|2m_X - m_{Z'}|$.

Among the different collider constraints the most effective ones are the ones which emerge from searches of dilepton resonances, even if the invisible decay channel for a Z' is taken into account. Using the invariant mass distribution of the heavy dilepton resonance, peaked at the Z' mass, one can discriminate the signal from the background nicely and for this reason the dilepton channel is considered to be a very good probe for these kinds of models.

As evidenced from the two top-row plots of figure 4 that these searches exclude most of the viable thermal DM region, leaving just a small portion of the parameter space around the Z' pole region. On the contrary, the impact of the mono-jet constraints is much more moderate and exists only for the light DM masses. The collider constraints, as already discussed, disappear very fast as the value of the kinetic mixing parameter δ decreases. For $\delta = 0.01$, (top-right panel of figure 4), compared to the $\delta = 0.1$ scenario, a much smaller portion of the parameter space remains excluded from the dileptons and mono-jet constraints. All the collider constraints disappear for $\delta = 0.001$ (bottom panel of figure 4) where the only constraint on the model parameter space comes from the requirement of the correct DM relic density.

III. SCENARIO-II: Z' - Z INTERACTION VIA A SECOND CHERN-SIMONS TERM

In this section, just like section II, we consider a CS term to connect a vectorial DM with a Z' . However, unlike section II the coupling between the Z' mediator and the neutral EW gauge bosons arises via a second independent CS term. Being guided by our previous approach, we will address the phenomenological implications of this setup as the result of a numerical scan over the free inputs after a brief illustration of the model followed by concise discussions on the constraints of correct relic density and different DM searches.

A. The Lagrangian

The Lagrangian describing the low-energy phenomenology of the aforementioned setup can be written as:

$$\mathcal{L} \supset \alpha_{\text{CS}} \epsilon^{\mu\nu\rho\sigma} X_\mu Z'_\nu X_{\rho\sigma} + \beta_{\text{CS}} \epsilon^{\mu\nu\rho\sigma} Z_\mu Z'_\nu B_{\rho\sigma} + \frac{m_{Z'}^2}{2} Z'^\mu Z'_\mu + \frac{m_X^2}{2} X^\mu X_\mu, \quad (28)$$

where α_{CS} and β_{CS} are the XXZ' and ZZZ' , $Z\gamma Z'$ coupling constants, respectively. $B_{\rho\sigma}$ denotes the field strength of the SM hypercharge gauge field. The origin of the coupling α_{CS} is the same

as of section II which will be discussed later in appendix B. The second CS coupling β_{CS} is non-invariant under the SM gauge group transformation. Nevertheless, as pointed out in ref. [48], it could be generated by considering the following gauge invariant effective operator obtained after integrating out some heavy degrees of freedom:

$$\mathcal{L} \propto i \epsilon^{\mu\nu\rho\sigma} D_\mu \theta_{Z'} \left((D_\nu H)^\dagger H - H^\dagger D_\nu H \right) B_{\rho\sigma}, \quad (29)$$

where $D_\mu \theta_{Z'} = \partial_\mu \theta_{Z'} - v_{Z'} q_{Z'} g_{Z'} Z'_\mu$ represents the covariant derivative of Stueckelberg axion $\theta_{Z'}$ while $D_\nu H$ denotes the usual covariant derivative of the SM-Higgs doublet. $q_{Z'}$, $v_{Z'}$ are the charge and VEV of the associated complex scalar field and Z'_ν is the gauge boson of the concerned $U(1)_{Z'}$ group with $g_{Z'}$ as the gauge coupling. After the EWSB and choosing unitary gauge for the $U(1)_{Z'}$ group (such that $\theta_{Z'}$, connected to the phase of an associated heavy Higgs field, gets "eaten" by the longitudinal component of Z'_μ), we recover the operator considered in eq. (28).

The structure of eq. (28) contains two CS couplings, namely α_{CS} and β_{CS} . The former is the same as of eq. (1) whose origin is explained in the appendix B while the latter appears from eq. (29). Given that the relevant charges are $\sim \mathcal{O}(1)$ (see eq. (B21)), the parameter α_{CS} from the associated pre-factor goes as $\sim \mathcal{O}(10^{-3})$. On the other hand, from eq. (29) the pre-factor for β_{CS} varies as $v_{Z'} v_h^2 / M^3$ with M as the cut-off scale of the theory, related to the mass of the associated heavy BSM fermions. Now assuming other relevant parameters as $\sim \mathcal{O}(1)$, even when $v_{Z'} \sim M$, one gets $\beta_{\text{CS}} \sim v_h^2 / M^2$. Hence, for $v_h \sim \mathcal{O}(10^2 \text{ GeV})$ and $M \sim \mathcal{O}(10 \text{ TeV})$ (this conservative limit is consistent with the hitherto undetected evidence of BSM physics at the 13 TeV LHC operation), $\beta_{\text{CS}} \sim \mathcal{O}(10^{-4})$ or $0.1 \times \alpha_{\text{CS}}$. It is thus apparent that in general a hierarchy between the values of two CS couplings is rather natural as they have two different theory origins. In our analysis we, however, also consider the possibility of $\alpha_{\text{CS}} = \beta_{\text{CS}}$.

B. Relic density

In the case of double CS terms, unlike the kinetic mixing scenario, the number of accessible DM pair annihilation channels is limited just to three options, i.e., $Z\gamma$, ZZ and $Z'Z'$. The first two are induced by s-channel exchange of the Z' while the third one is induced by t/u channel exchange of a DM state. Simple analytical approximations of the corresponding DM pair annihilation cross-sections can be derived, as usual, through the customary velocity expansion:

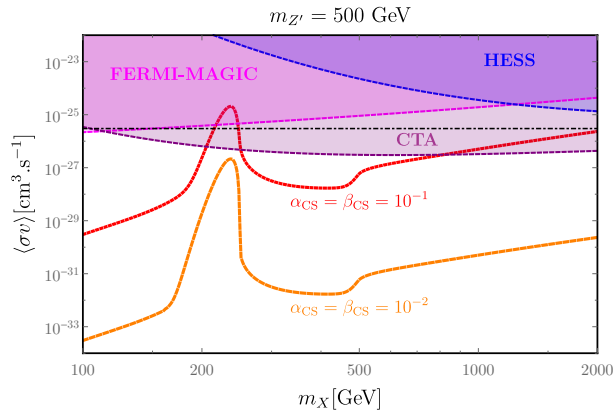


Figure 5. Thermally averaged DM pair annihilation cross-section at the time of thermal freeze-out, in the presence of double CS terms, as function of the DM mass m_X , for $m_{Z'} = 500 \text{ GeV}$ and two assignments for α_{CS} and β_{CS} , namely $\alpha_{\text{CS}} = \beta_{\text{CS}} = 0.1$ (red coloured curve) and $\alpha_{\text{CS}} = \beta_{\text{CS}} = 0.01$ (orange coloured curve). The black coloured dashed line represents the thermally favored value of $\langle\sigma v\rangle = 3 \times 10^{-26} \text{ cm}^3 \text{ s}^{-1}$. Different exclusion regions are the same as of figure 1.

- $XX \rightarrow Z\gamma$:

$$\langle\sigma v\rangle_{Z\gamma} \simeq \frac{\alpha_{\text{CS}}^2 \beta_{\text{CS}}^2 c_W^2 (4m_X^2 - m_Z^2)^3}{48\pi m_X^4 m_{Z'}^4} \frac{1}{x}, \quad \text{for } m_Z \ll m_X. \quad (30)$$

- $XX \rightarrow ZZ$:

$$\langle\sigma v\rangle_{ZZ} \simeq \frac{8\alpha_{\text{CS}}^2 \beta_{\text{CS}}^2 s_W^2 (m_X^2 - m_Z^2)^{3/2}}{3\pi m_X m_{Z'}^4} \frac{1}{x}, \quad \text{for } m_Z \ll m_X. \quad (31)$$

- $XX \rightarrow Z'Z'$:

$$\langle\sigma v\rangle_{Z'Z'} \simeq \frac{\alpha_{\text{CS}}^4 (32m_X^8 + 14m_{Z'}^8 - 56m_X^6 m_{Z'}^2 + 69m_X^4 m_{Z'}^4 - 50m_X^2 m_{Z'}^6)}{9\pi m_X^2 m_{Z'}^4 (m_{Z'}^2 - 2m_X^2)^2} \sqrt{1 - \frac{m_{Z'}^2}{m_X^2}}, \quad \text{for } m_{Z'} \ll m_X. \quad (32)$$

The behavior of the DM pair annihilation cross-section, as function of its mass, is reported in figure 5. Similar to the scenario discussed in section II, the DM pair annihilation cross-sections are typically velocity suppressed except the s-wave annihilation channel into $Z'Z'$ final states. As evidenced from figure 5 that value of the thermally averaged DM pair annihilation cross-section can match the experimentally favored value only at $m_X \sim \frac{m_{Z'}}{2}$, (i.e., pole region), and for $m_X > m_{Z'}$, so that the DM pair annihilation into Z' pairs is allowed. Furthermore, to avoid overproduction of the DM, α_{CS} values at least $\sim \mathcal{O}(0.1)$ are needed.

C. Indirect detection

Possible prospects of ID rely, as the kinetic mixing scenario, mostly on the detection of gamma-rays produced after the DM pair annihilation into Z' pairs which subsequently decay into hadrons. Indeed the other two annihilation channels, i.e., ZZ and $Z\gamma$ have p-wave (velocity dependent) annihilation cross-sections lying several orders of magnitude below the present and the near future experimental sensitivities [122–135].

That said, similar to the previous case, we assumed that the annihilations into Z' pairs lead to a gamma-ray yield comparable to the W^+W^- final state. Therefore, one can use CTA sensitivity to DM annihilations into the W^+W^- channel to constrain the model as can be seen in figure 5. It is clear that only CTA is expected to mildly probe this setup for DM masses above 1 TeV.

D. Direct Detection

In the case of double CS interactions, the Z' has no direct/tree-level couplings with the SM-quarks (or the gluons) and hence, no operators relevant for DD is induced at the tree-level.

E. Collider phenomenology

In the scenario with double CS interactions, the Z' is directly coupled only with the Z -boson and the photon. Tree level production of the Z' at the LHC, nevertheless, is possible through vector boson fusion (VBF) in association with two hadronic jets. The production cross-section, however, is more suppressed compared to the case of a single CS interaction with kinetic mixing (see section II) which has direct couplings with quarks at the tree level ⁸.

We have reported in figure 6 the expected Z' production cross-section at the LHC for 13 TeV centre-of-mass energy as a function of the mass of Z' ($m_{Z'}$) for three values of parameter $\beta_{CS} = 0.5, 0.1$ and 0.01 , depicted with solid red coloured line, dashed blue coloured line and dot-dashed orange coloured line, respectively. The cross-section has been computed using the procedure illustrated in ref. [139] where discovery prospects of a Z' , produced via Z -fusion and decaying to four leptons final states, i.e., $Z' \rightarrow ZZ \rightarrow 4l$, have been investigated. These kinds of signals could be probed at the LHC with 14 TeV centre-of-mass energy provided that $\sigma(pp \rightarrow Z') \simeq 1$ pb. It is now apparent from figure 6 that a future Z' discovery would appear feasible only for $\beta_{CS} \simeq 0.5$ with

⁸ A richer collider phenomenology could appear in extensions of the proposed scenario in which the Z' has direct coupling with the W -boson and the gluons as studied in refs. [49, 66, 136–138].

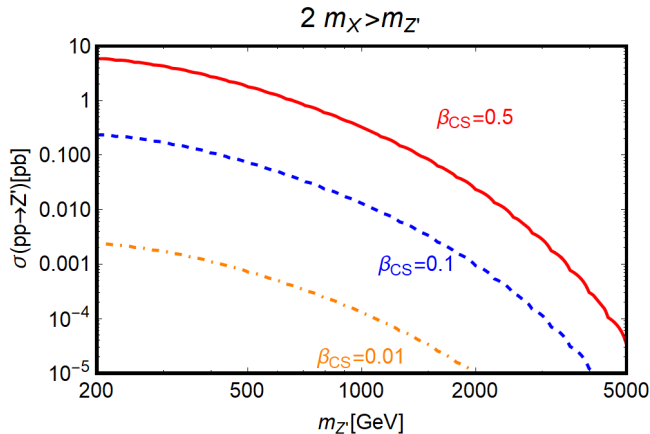


Figure 6. Production cross-section of the Z' at the LHC through VBF as a function of $m_{Z'}$ for 13 TeV centre-of-mass energy for three different values of β_{CS} parameter, namely, 0.5, 0.1 and 0.01 that are represented with solid red, dashed blue and dot-dashed orange coloured lines, respectively. The choice of $2m_X > m_{Z'}$ forbids invisible decay of the Z' .

$m_{Z'} \lesssim 1$ TeV. For lower values of β_{CS} the production cross-section, goes as β_{CS}^2 , would appear very suppressed to escape detection at the LHC unless (possibly) one considers higher luminosity. One should, however, remain careful about $\sim \mathcal{O}(1)$ value of the parameter β_{CS} as this would indicate a scale for the associated heavy fermion mass M (see discussions after eq. (29)) well within the reach of ongoing LHC operation where, unfortunately, no evidence of BSM physics has been confirmed till date.

Notice that in the above discussion we have implicitly assumed that invisible decay of the Z' is kinematically forbidden, i.e., $2m_X > m_{Z'}$. If this was not the case, the production cross-section of $4l + 2j$ final states would be suppressed further by the non-zero invisible branching fraction of the Z' . On the other hand, a sizable invisible branching fraction for Z' might offer meaningful detection prospects for $pp \rightarrow Z' \rightarrow XX + 2j$ process. Investigation of such signature would require a dedicated study which is beyond the scope of this work.

F. Results

Similar to the first model considered in this work, we perform a scan in the parameter space over α_{CS} , β_{CS} , $m_{Z'}$ and m_X and represent our findings in figure 7 showing the phenomenologically viable model points. One should note that, contrary to the kinetic mixing scenario, the absence of tree-level Z' couplings with the SM fermions appears useful to efface a set of constraints coming

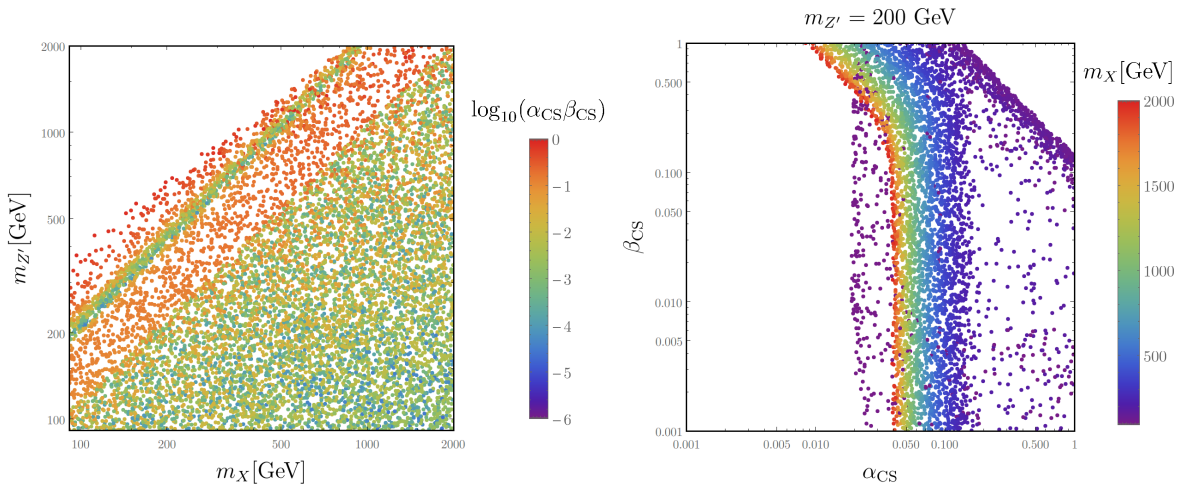


Figure 7. Results of a parameter scan for the setup with two CS terms showing points compatible with the DM phenomenology. The left plot is in $m_X, m_{Z'}$ bi-dimensional plane with a colour coding for the product of two CS couplings $\alpha_{CS}\beta_{CS}$ while the right plot is in α_{CS}, β_{CS} plane for $m_{Z'} = 200 \text{ GeV}$ with a colour coding for various m_X values.

from the precision Z -physics and collider observations. The scan is performed in the following ranges:

$$\alpha_{CS} \in [10^{-3}, 1], \quad \beta_{CS} \in [10^{-3}, 1], \quad m_X \in [90 \text{ GeV}, 2 \text{ TeV}], \quad m_{Z'} \in [90 \text{ GeV}, 2 \text{ TeV}]. \quad (33)$$

As expected, the left panel of figure 7, representing the viable model points in the bi-dimensional plane $(m_X, m_{Z'})$, shows, similar to the kinetic mixing scenario, a sensitive preference for configurations with $m_X > m_{Z'}$, for which the correct relic density can be more easily achieved through the velocity unsuppressed annihilation rate into Z' pairs. This is further evidenced by the right panel of figure 7, investigating the bi-dimensional plane $(\alpha_{CS}, \beta_{CS})$ for a fixed $m_{Z'}$. Indeed, most of the points approximately trace isocontours with a shape independent of β_{CS} , unless this coupling is much bigger than α_{CS} . This behavior would be exactly expected in the case when the DM relic density is mostly accounted by the annihilation into the $Z'Z'$ final state since the corresponding rate depends only on α_{CS} (see eq. (32)). One must note that the demand of $\beta_{CS} \gg \alpha_{CS}$ is theoretically challenging since normally one would expect $\beta_{CS} < \alpha_{CS}$ as already discussed in the context of eq. (29).

It is curious to note the apparent conflicts among the DM detection prospects in DD, ID and collider experiments with Z' searches at the collider and theoretical consistency of the studied framework. For example, from figure 6 it is evident that a Z' discovery at the LHC with 13 TeV

centre-of-mass energy would require $\beta_{\text{CS}} \sim \mathcal{O}(1)$ and $m_{Z'} \lesssim 1$ TeV. Such high value of β_{CS} , as already mentioned, is hard to accommodate phenomenologically. Pushing β_{CS} towards its natural regime, i.e., $\sim \mathcal{O}(10^{-4})$, on the other hand, would predict a $\alpha_{\text{CS}} \sim \mathcal{O}[10 - 10^4]$ to retain some of the viable points, notably for $\log_{10}(\alpha_{\text{CS}}\beta_{\text{CS}}) \gtrsim -3$, as shown in the left plot of figure 7 to respect the DD, ID and relic density constraints. Now keeping in mind the radiative origin of α_{CS} , as explained in the appendix B, such high values of α_{CS} would require either a pathologically behaved strongly coupled theory or unnatural high values for the associated charges. Lower and rather natural α_{CS} values, e.g., $\sim 10^{-3}$, can ameliorate such theoretical shortcomings and one can still get viable points consistent with the DM observables in the region of $\log_{10}(\alpha_{\text{CS}}\beta_{\text{CS}}) \lesssim -5$. The associated low β_{CS} values, however, failed to produce detectable Z' signals at the LHC as already shown in figure 6. Similar contradictions also appear for the right plot of figure 7 which, keeping in mind the collider detection prospect of a Z' , predicts $0.01 \lesssim \alpha_{\text{CS}} \lesssim 0.3$ for $m_{Z'} = 200$ GeV. This range of the parameter α_{CS} once again either requires moderate values of the involved charges or asks for a strongly coupled model frameworks. In a nutshell, keeping in mind the detection possibilities of the BSM physics, either in DM or in collider searches, together with an elegant theoretical construction, the scenario with two CS interactions is less appealing compared to a scenario with one CS interaction and a kinetic mixing. Such simple conclusion, however, is not obvious when a scenario with two CS interactions involves non-Abelian gauge groups.

IV. ORIGIN OF A CHERN-SIMONS COUPLING AND UV COMPLETION

In this section we propose a UV complete model that can address the origin of CS and kinetic mixing terms. The generation of a generalized CS interaction term between the gauge boson of a BSM $U(1)$ group and the SM gauge bosons has already been proposed in refs. [46, 50, 136]. The effective CS coupling is originated from the triangle loops involving BSM heavy fermions, charged under both the SM $U(1)_Y$ and a BSM $U(1)$ symmetry groups, after integrating out the heavy degrees of freedom. In this work we consider a similar construction where a CS interaction term is generated between the gauge bosons of two new BSM symmetry groups labeled as $U(1)_X$ (associated to the DM) and $U(1)_V$ (associated with \tilde{V}_μ), respectively ⁹.

Concerning the origin of kinetic mixing, in the most general scenario, i.e., when the new BSM fermions are charged ¹⁰ under the BSM gauge groups $U(1)_X$, $U(1)_V$ as well as with respect to $U(1)_Y$

⁹ For the convenience of reading note that in scenario-I, \tilde{V}_μ denotes the gauge field of $U(1)_V$ which, after diagonalization of the flavour basis Lagrangian, is written as Z'_μ while in scenario-II the kinetic and mass terms are already diagonalized and hence, $\tilde{V}_\mu = Z'_\mu$.

¹⁰ One could expect the BSM fermions to have an impact on the DM decoupling process from the SM thermal bath,

of the SM, one can radiatively generate three possible kinetic mixing terms like $X^{\mu\nu}\tilde{V}_{\mu\nu}$, $X^{\mu\nu}B_{\mu\nu}$ and $\tilde{V}^{\mu\nu}B_{\mu\nu}$ with ¹¹ appropriate field strengths of the involved Abelian groups. The co-efficients for these terms emerge as a result of integrating out the aforesaid heavy BSM fermionic degrees of freedom and also include associated gauge charges. One should remain careful at this stage as a kinetic mixing like $X^{\mu\nu}B_{\mu\nu}$ triggers a mixing between the DM X_μ and Z_μ which would subsequently allow the DM to decay into the SM fermions and thereby, spoiling its stability. A similar situation can also appear for $X^{\mu\nu}\tilde{V}_{\mu\nu}$, given that \tilde{V}_μ is somehow, e.g., via a second kinetic mixing $\tilde{V}^{\mu\nu}B_{\mu\nu}$, decaying into the SM particles. It is thus important to assign gauge charges for the BSM fermions in an elegant way such that the stability of the DM remains preserved.

We denote new BSM fermions as χ (ψ), chiral with respect to $U(1)_X$ ($U(1)_V$) while vector like compared to $U(1)_V$ ($U(1)_X$) as well as to the SM [136]. This way no new chiral anomalies are introduced in the SM while one can find suitable charge assignments for these BSM fermions to efface new anomalies. Regarding the mass generation of these new fermions the most plausible option is represented via Yukawa interactions with two BSM complex scalar fields $\phi_{X,V}$. The relevant Lagrangian is written as:

$$\mathcal{L}^{\text{fermions}} = -y_F\phi_V\bar{\psi}_{1L}\psi_{1R} - y_F\phi_V^*\bar{\psi}_{2L}\psi_{2R} - y_F\phi_X\bar{\chi}_{1L}\chi_{1R} - y_F\phi_X^*\bar{\chi}_{2L}\chi_{2R} + \text{h.c.}, \quad (34)$$

where y_F represents generic Yukawa couplings ¹². The complex scalar fields ϕ_X , ϕ_V can be written using the following parametrization as:

$$\phi_X = (v_X + h_X)e^{i\theta_X/v_X} \quad \text{and} \quad \phi_V = (v_V + h_V)e^{i\theta_V/v_V}, \quad (35)$$

with v_X , v_V and h_X , h_V denoting the corresponding VEVs and the Higgs fields. Here θ_X , θ_V are Stueckelberg axions [140–142]. Investigating the kinetic terms for these scalars with suitable BSM covariant derivatives, one gets, for example, for ϕ_X :

$$|D_\mu\phi_X|^2 = |\partial_\mu\phi_X - iq_X g_X \phi_X X_\mu|^2 \supset (\partial_\mu\theta_X - q_X g_X v_X X_\mu)^2, \quad (36)$$

with g_X as the gauge coupling of the $U(1)_X$ gauge group and q_X as the charge of ϕ_X with respect to this group. The DM mass thus, is generated via the Stueckelberg mechanism [140–142]. The masses

however, since the freeze out occurs only when the DM particles are non-relativistic, the BSM fermions would have already decoupled and their density would be exponentially suppressed due to Boltzmann factor.

¹¹ Such terms, being Lorentz invariant, renormalizable and invariant under the SM gauge groups, can directly appear in Lagrangian. We, however, do not consider such possibility and confine our discussion on scenarios where such interactions are radiatively generated.

¹² We, without the loss of generality, consider identical Yukawa couplings for all the BSM fermions for simplicity since the final results are independent of them.

	ψ_{1L}	ψ_{1R}	ψ_{2L}	ψ_{2R}	χ_{1L}	χ_{1R}	χ_{2L}	χ_{2R}
$U(1)_X$	e_1	e_1	e_2	e_2	e_4	e_3	e_3	e_4
$U(1)_V$	q_1	$-q_1$	$-q_1$	q_1	q_2	q_2	$-q_2$	$-q_2$

Table I. Charge assignments of the left- and right- chiral components of the BSM fermions which belong to gauge group $U(1)_X \times U(1)_V$.

for the new BSM fermions, χ_1, χ_2 , are also generated after the spontaneous symmetry breaking (SSB) in the $U(1)_X$ sector. In fact, after SSB one ends up with the following tree-level realizations for various masses:

$$m_{h_X} \sim \sqrt{\lambda_X} v_X, \quad m_F \sim y_F v_X, \quad m_X \sim g_X q_X v_X, \quad (37)$$

where λ_X is the quartic coupling of the ϕ_X potential and the notation m_F is used to represent generic BSM fermion masses. A similar construction holds for $U(1)_V$ with $\lambda_V, g_V, q_V, m_{h_V}$ and m_V as the appropriate replacements. We further consider the following hierarchy among the various couplings: $\lambda_X, \lambda_V \gg y_F \gg g_X, g_V$. Such choice implies $m_{h_X}, m_{h_V} \gg m_F \gg m_X, m_V$ for $\lambda_X, g_X \sim \lambda_V, g_V$ with $v_X \sim v_V$. Hence, at an energy scale $E \sim m_F \ll m_{h_X}, m_{h_V}$, the new scalars h_X, h_V are nearly decoupled from the theory given that v_X, v_V are reasonably high. In this limit one can use the following approximations $\phi_X \simeq v_X e^{i\theta_X/v_X} \simeq v_X + i\theta_X$ and $\phi_V \simeq v_V e^{i\theta_V/v_V} \simeq v_V + i\theta_V$ which help to recast eq. (34) as:

$$\mathcal{L}^{\text{fermions}} \supset -iy_F \theta_V \bar{\psi}_1 \gamma_5 \psi_1 + iy_F \theta_V \bar{\psi}_2 \gamma_5 \psi_2 - iy_F \theta_X \bar{\chi}_1 \gamma_5 \chi_1 + iy_F \theta_X \bar{\chi}_2 \gamma_5 \chi_2. \quad (38)$$

The structure of Yukawa couplings of the new fermions, as well as the requirement of anomaly cancellations, restrict the possible charge assignments under the BSM $U(1)$ groups. A set of assignments complying with these two requirements is reported in table I. As evident from table I that this kind of charge assignments allows natural cancellations of the $U(1)_{V,X}^3$ anomalies, independently for the ψ and χ sectors, irrespective of the values of q_i, e_i charges¹³.

The cancellation of the mixed anomalies, e.g., $U(1)_V U(1)_X^2$, is instead achieved in a non-trivial way. This, indeed, requires the following relation between the charges:

$$q_2 = \frac{q_1(e_1^2 - e_2^2)}{(e_3^2 - e_4^2)}. \quad (39)$$

¹³ One could see from table I that the sum of all left- and right-chiral charges for ψ and χ vanishes for $U(1)_V$ while for $U(1)_X$ it is $2 \sum_{i=1}^4 e_i$. If we also set this sum to be zero, as expected from the requirement of gauge-gravity anomaly cancellation for an Abelian group, we can recast eq. (39) as $q_2 = \frac{q_1(e_2 - e_1)}{e_3 - e_4}$.

Further, the charge assignments of table I predicts a vanishing kinetic mixing between X and V as

$$\sum_{\xi=\psi_i, \chi_i}^{i=1,2} c_{\xi_L}^X c_{\xi_L}^V + c_{\xi_R}^X c_{\xi_R}^V = 0, \quad (40)$$

with $c_{\xi_{L(R)}}^{X(V)}$ representing appropriate charges shown in the table I. This, as discussed already, is crucial since a mixing between X and V , in the presence of a kinetic mixing between V , Z , can trigger a subsequent mixing between X and Z , such that X can decay into the SM fermions and thereby, the stability of the DM gets spoiled.

We show in detail later in appendix B that when eq. (39) is satisfied, it appears feasible to construct an anomaly free theory where the following effective operator emerges after integrating out heavy fermionic degrees of freedom from the triangular loops:

$$\epsilon^{\mu\nu\rho\sigma} D_\mu \theta_X D_\nu \theta_V X_{\rho\sigma}, \quad (41)$$

where θ_X , θ_V are Stueckelberg axions of the $U(1)_X$, $U(1)_V$ groups and $D_\mu \theta_X = \partial_\mu \theta_X - g_X q_X v_X X_\mu$, and $D_\nu \theta_V = \partial_\nu \theta_V - g_V q_V v_V \tilde{V}_\nu$ with X_μ , \tilde{V}_ν as gauge bosons of the concerned $U(1)_X$, $U(1)_V$ groups, respectively. Eq. (41) is invariant under the following gauge transformations:

$$X_\mu \rightarrow X_\mu + \partial_\mu \alpha_X, \quad \tilde{V}_\mu \rightarrow \tilde{V}_\mu + \partial_\mu \alpha_V, \quad \theta_X \rightarrow \theta_X + g_X q_X v_X \alpha_X, \quad \theta_V \rightarrow \theta_V + g_V q_V v_V \alpha_V, \quad (42)$$

with α_X and α_V as the transformation parameters. The same equation, after considering unitary gauge, leads to the following operator as introduced earlier in eq. (1):

$$\mathcal{L} = \alpha_{\text{CS}} \epsilon^{\mu\nu\rho\sigma} X_\mu \tilde{V}_\nu X_{\rho\sigma}, \quad (43)$$

with

$$\alpha_{\text{CS}} \equiv \frac{q_1 (e_2^2 - e_1^2)}{8\pi^2}. \quad (44)$$

One can define an effective charge $\tilde{Q}^3 \equiv q_1 (e_2^2 - e_1^2)$ to get a simple relation:

$$\alpha_{\text{CS}} = \frac{\tilde{Q}^3}{8\pi^2}. \quad (45)$$

Clearly $\alpha_{\text{CS}} \sim \mathcal{O} [10^{-2}, 1]$ (see eq. (27)) or $\sim \mathcal{O} [10^{-3}, 1]$ (see eq. (33)) corresponds to a $\sim \mathcal{O}(1)$ value of the effective charge \tilde{Q} for one generation of the BSM fermions.

Note that the CS coupling α_{CS} has no explicit dependence on the BSM fermion mass, i.e., it seems to remain finite as m_F , the relevant heavy fermion mass, $\rightarrow \infty$ and thereby, resembles

a non-decoupling effect. This is a consequence of the assumption $\lambda_X, \lambda_V \gg y_F \gg g_X, g_V$, as considered earlier, which makes α_{CS} independent of m_F as long as $m_F \gg m_X, m_{Z'}$ such that the adopted effective approach remains justified for an energy scale E below the mass of the “lightest” BSM fermion of the theory. The parameter β_{CS} (see eq. (29)), on the contrary, vanishes as the associated BSM fermion masses $\rightarrow \infty$, as expected according to the decoupling effect.

One should further note that as the effective charge \tilde{Q} includes the gauge couplings in its definition, $\tilde{Q} \sim \mathcal{O}(1)$ implies either $g_X \sim g_V \sim \mathcal{O}(1)$ or a large multiplicity of the BSM fermions having gauge charges $\sim \mathcal{O}(1)$. However, as mentioned previously, the aforementioned theoretical construction relies on the assumption of $\lambda_X, \lambda_V \gg g_X, g_V$ which, for $g_X, g_V \sim \mathcal{O}(1)$, hints towards a strongly coupled theory. In this regime one would encounter several theoretical issues like the vacuum instability, etc. which might spoil viability of the effective approach. Further discussions of such issues are beyond the theme of this paper and we note in passing that from the view point of a radiative origin, $\alpha_{\text{CS}} \sim \mathcal{O}(1)$ is unnatural.

The kinetic mixing parameter δ (see eq. (1)), as already stated in the beginning of this section, can get generated at the loop level from two sets of the BSM fermions (preferably vector-like to avoid new anomalies in a trivial way) charged under the SM $U(1)_Y$ and BSM $U(1)_V$ groups and having masses M_y and M_v , respectively. The parameter δ is then estimated as $\simeq (q_Y g_Y q_V g_V / 16\pi^2) \times \log(M_v/M_y)$ [42] with q_Y, q_V, g_Y, g_V as the relevant combination of gauge charges and gauge couplings of the associated gauge groups. Assuming these gauge charges and couplings, as well as $\log(M_v/M_y)$, to be $\sim \mathcal{O}(1)$, one would expect natural range of δ as $\sim \mathcal{O}(10^{-3} - 10^{-2})$. This range, as evident from eq. (44) and eq. (B21), is almost the same as of α_{CS} , considering $\sim \mathcal{O}(1)$ values of the involved gauge charges. Both these natural ranges of CS coupling α_{CS} and kinetic mixing parameter δ are connected with their radiative origins.

V. SUMMARY AND CONCLUSIONS

In this article we scrutinized experimental viability and theoretical consistency of the WIMP DM models comprised of an Abelian vectorial DM X_μ and an Abelian Z' portal, coupled through a CS interaction. We studied two possibilities of connecting the Z' with the SM: (1) via a kinetic mixing with the SM hypercharge field strength and, (2) another CS coupling with Z boson and field strength of the SM $U(1)_Y$ group. We successively addressed the DM and collider phenomenologies of these two scenarios. Regarding the DM phenomenologies we investigated the detection prospects of these two frameworks in the light of accommodating the correct relic density and sensitivity

reaches of the various existing as well as anticipated upcoming DD and ID experiments. Concerning collider probes we examined the observational aspects of these models from the view point of dijet, dilepton resonances and mono- \mathbf{X} searches using the 13 TeV LHC data. Further, we also studied the viable ranges of the associated parameters focusing on the possible theoretical and/or “well-measured” experimental constraints, mainly for the kinetic mixing scenario, arising from the EWPT, ρ -parameter, Z -mass, total and invisible Z -decay widths, etc. Finally, we also explored possible origins of a kinetic mixing term and a CS interaction term, arising via a set of heavy BSM fermions running in the triangle loops, from the standpoint of an UV complete theory. These fermions are charged under the new BSM gauge groups, connected with the Abelian DM and the Z' , and possess non-trivial charges (or vector-like) with respect to the SM. We explained how a specific choice of the associated charges for these fermions can appear instrumental to acquire a CS coupling, a kinetic mixing term for Z - Z' , an anomaly free model setup and the DM stability.

Given that X_μ is the “only” DM candidate, one observes that the DM experimental detection/exclusion potentials (correct relic density and sensitivities towards DD, ID experiments), for the model with one CS coupling and a kinetic mixing, appear promising for $m_{Z'}$ preferably below 1 TeV with $m_X \geq m_{Z'}$ configuration, expect the pole region (i.e., $2m_X \simeq m_{Z'}$), for $\delta \sim \mathcal{O}(0.1)$, $\mathcal{O}(0.1) \lesssim \alpha_{\text{CS}} \sim \mathcal{O}(1)$. Such ranges for δ , α_{CS} parameters as well as low $m_{Z'}$ are noticed to be incompatible with the collider searches of heavy dilepton resonances and mono- \mathbf{X} events. One can, of course, lower the value of parameter $\delta \sim \mathcal{O}(10^{-3})$ to efface the existing collider constraints. Such values of δ would predict $\lesssim \mathcal{O}(1)$ events even if one considers high-luminosity run of the LHC or future proton-proton colliders with higher centre-of-mass energies and thus, conceal the model from collider searches till a faraway future. As a quantitative example, to get $\sim \mathcal{O}(10)$ events for TeV scale new physics, i.e., $m_{Z'} = 1$ TeV, from $pp \rightarrow Z' \rightarrow jj, l^+l^-$ processes at the 100 TeV proton-proton collider, assuming a “100%” detection efficiency, one would require 100 fb^{-1} of integrated luminosity to probe the $\delta = 10^{-3}$ configuration. The situation is similarly disappointing concerning the DM phenomenology with such δ values, unless sensitivity reaches of the relevant DD, ID experiments are improved by several orders of magnitude and the idea of multi-component DM is invoked to account for the correct relic density. One should note that $\delta \lesssim 10^{-3}$ and hence, the resultant suppressed Z - Z' mixing, can peacefully co-exist with the constraints of EWPT, ρ -parameter and the measured Z -boson mass and decay (total, invisible¹⁴) widths. In a nutshell, we see that δ value in the ball park of 10^{-3} appears experimentally unpleasant. Nevertheless, assigning a radiative origin to this coupling, involving heavy BSM fermions, $\delta \lesssim \mathcal{O}(10^{-3})$ is the natural

¹⁴ Depends also on α_{CS} and irrelevant for $2m_X > m_{Z'}$.

range that one would expect for the parameter δ , unless a high multiplicity of the associated BSM fermions is considered to raise this parameter (at least) by one order of magnitude that makes the chosen setup testable at the ongoing and upcoming experiments. For example, with $\delta = 0.01$, a 1 TeV Z' can produce $\sim \mathcal{O}(10)$ “detectable” events in dijet/dilepton resonance searches itself at the 13 TeV LHC with about 100 fb^{-1} of integrated luminosity, even assuming a “10%” detection efficiency. A radiative origin for CS coupling α_{CS} , from the perspective of an UV complete construction, also predicts a natural range for α_{CS} as $\lesssim \mathcal{O}(10^{-3})$ whereas discovery/exclusion prospects, with the existing and near future experimental setups, favour $\alpha_{\text{CS}} \sim \mathcal{O}(1)$. Such α_{CS} values, along with a δ of similar order, can accommodate the correct relic density rather easily and can be probed/excluded from DD, ID and collider (via mono- \mathbf{X}) searches. An $\mathcal{O}(1)$ value of α_{CS} , just like the kinetic mixing parameter δ , is hard to explain with a radiative origin unless more families of the BSM fermions are included. Any such non-minimal constructions, i.e., large number of BSM fermions to increase δ and/or α_{CS} value(s) or a multi-component DM to account for the correct relic density with “natural” δ values would reduce the model predictivity. Moreover, the underlying assumptions behind the UV complete construction of a CS coupling can easily lead to a strongly coupled theory where the validity of the adopted effective approach might seem questionable.

Experimental attainments of the second case study with two CS couplings are more contrived due to the absence of a tree-level mixing between the Z' and the SM fermions, unlike the first case study with one CS coupling and a kinetic mixing. Missing tree-level couplings between Z' and the SM fermions conceal this framework from constraints like the EWPT, ρ -parameter, precision Z physics, etc. which offer notable effects on the model parameter space for scenario-I. In this framework, DD prospects are missing at the tree-level and ID sensitivities remain orders of magnitude below the ongoing and upcoming experimental reaches. The requirement of the correct relic density, except the pole region, is possible for $m_X > m_{Z'}$ with $\alpha_{\text{CS}}, \beta_{\text{CS}} \gtrsim \mathcal{O}(0.1)$ even at low $m_{Z'}$. This regime of the two CS coupling values is resourceful for a LHC detection, although the high-luminosity run appears to be the preferred choice. The collider discovery/exclusion potentials are primarily sensitive to β_{CS} except when one considers invisible decay of the Z' (i.e., mono- \mathbf{X} searches) where α_{CS} also enters in the analysis. The experimentally favoured ranges of the two CS coupling values, just like the kinetic mixing scenario, are hard to realize from their respective theoretical origins. The conclusion for α_{CS} remains the same as of the kinetic mixing scenario, since it possesses the same radiative origin involving heavy BSM fermions from the standpoint of an UV complete construction. The origin of the second CS coupling β_{CS} is also connected to the BSM fermions, however, in a more convoluted way that allows a vanishing value for β_{CS} as the associated fermions masses get

heavier and decouple from the low-energy theory. Further, by construction, in general one expects $\alpha_{CS} > \beta_{CS}$ which indicates natural range of β_{CS} in the ballpark of 10^{-4} . Thus, this scenario remains practically hidden from the collider searches, even considering the high-luminosity LHC or a 100 TeV proton-proton collider. The latter, being quantitative, would require a 1000 fb^{-1} of integrated luminosity to yield $\sim \mathcal{O}(1)$ events for a 1 TeV Z' with $\beta_{CS} = 10^{-4}$, assuming a “100%” detection efficiency. The requirement of the correct relic density also faces similar hindrance. The trick of pushing β_{CS} values upwards by adding more BSM fermions is rather intricate compared to the kinetic mixing scenario.

The key outcomes of this study, based on the obtained results, give the following conclusions: (1) scenario-II with two CS couplings, both connected to some Abelian groups, would appear rather hard to probe experimentally even in the near future experiments if one sticks to a theoretically “well-behaved” construction. Moving to a setup where the second CS coupling is connected to some non-Abelian groups, for example, bridging an Abelian Z' with gluons, one can efface such limitations and the concerned scenario could produce detectable signals at the DM and the collider experiments. (2) Phenomenological viability of scenario-I with one CS coupling and a kinetic mixing, together with an UV complete model construction, also faces challenges to comply with the relevant experimental search sensitivities, however, in a lessened way. In particular, $\mathcal{O}(10^{-3}) \lesssim \delta \lesssim \mathcal{O}(10^{-2})$ configuration with $m_{Z'}$ around a TeV could be probed at the 14 TeV LHC with full luminosity as well as in high-luminosity LHC or in the next generation proton-proton colliders with increased centre-of-mass energies. The DD, ID prospects, with naturally preferred α_{CS} values, however, still remain well beyond the reaches of the next generation experiments although the requirement of the correct relic density can be accounted for by adding other DM candidates.

ACKNOWLEDGEMENTS

The authors would like to thank A. Pukhov and B. Fuks for substantial help with MicrOmegas and FeynRules, E. Dudas, G. Bhattacharyya, H.M. Lee, E. Kuffik, Y.Hochberg and H. Murayama, for enlightful discussions. P. G. acknowledges the support from P2IO Excellence Laboratory (LABEX). This work is also supported by the Spanish MICINN’s Consolider-Ingenio 2010 Programme under grant Multi-Dark **CSD2009-00064**, the contract **FPA2010-17747**, the France-US PICS no. 06482 and the LIA-TCAP of CNRS. Y. M. acknowledges partial support from the ERC advanced grants Higgs@LHC and MassTeV and from the European Union’s Horizon 2020 research and innovation (programme under the Marie Skłodowska-Curie grant agreements No 690575 and

No 674896). This research was also supported in part by the Research Executive Agency (REA) of the European Union under the Grant Agreement **PITN-GA2012-316704** ("HiggsTools") and by the CEFIPRA Project No. 5404-2: "Glimpses of New Physics".

Appendix A: Decay widths of the Z' boson

a. Kinetic mixing scenario

$$\Gamma_{XX} = \frac{(g_X^{Z'})^2 \sqrt{\frac{m_{Z'}^2}{4} - m_X^2} (m_{Z'}^2 - 4m_X^2)^2}{48\pi m_X^2 m_{Z'}^2}. \quad (\text{A1})$$

$$\Gamma_{Zh} = \frac{(g_{hZ Z'})^2 \left(-2m_{Z'}^2 (m_h^2 - 5m_Z^2) + (m_h^2 - m_Z^2) 2 + m_{Z'}^4 \right) \sqrt{\frac{(-m_h^2 + m_Z^2 + m_{Z'}^2)^2}{4m_{Z'}^2} - m_Z^2}}{96\pi m_Z^2 m_{Z'}^4}. \quad (\text{A2})$$

$$\Gamma_{\bar{f}f} = n_c \frac{\sqrt{\frac{m_{Z'}^2}{4} - m_f^2} \left[m_f^2 \left(2(v_f^{Z'})^2 - 4(a_f^{Z'})^2 \right) + m_{Z'}^2 \left((a_f^{Z'})^2 + (v_f^{Z'})^2 \right) \right]}{6\pi m_{Z'}^2}, \quad (\text{A3})$$

where n_c denotes the colour factor, equals to 3 for quarks and 1 for leptons. $a_f^{Z'} = \frac{g_{fR}^{Z'} - g_{fL}^{Z'}}{2}$ and $v_f^{Z'} = \frac{g_{fR}^{Z'} + g_{fL}^{Z'}}{2}$ are the axial and vector couplings respectively.

$$\Gamma_{W^+W^-} = \frac{(g_W^{Z'})^2 \sqrt{\frac{m_{Z'}^2}{4} - m_W^2} (-68m_W^4 m_{Z'}^2 + 16m_W^2 m_{Z'}^4 - 48m_W^6 + m_{Z'}^6)}{96\pi m_W^4 m_{Z'}^2}. \quad (\text{A4})$$

b. Two Chern-Simons couplings scenario

$$\Gamma_{XX} = \frac{\alpha_{\text{CS}}^2 (m_{Z'}^2 - 4m_X^2)^2 \sqrt{m_{Z'}^4 - 4m_X^2 m_{Z'}^2}}{24\pi m_X^2 m_{Z'}^3}. \quad (\text{A5})$$

$$\Gamma_{Z\gamma} = \frac{\beta_{\text{CS}}^2 \cos^2 \theta_W (m_{Z'}^2 - m_Z^2)^3 (m_{Z'}^2 + m_Z^2)}{24\pi m_Z^2 m_{Z'}^5}. \quad (\text{A6})$$

$$\Gamma_{ZZ} = \frac{\beta_{\text{CS}}^2 \sin^2 \theta_W (m_{Z'}^2 - 4m_Z^2)^2 \sqrt{m_{Z'}^4 - 4m_Z^2 m_{Z'}^2}}{24\pi m_Z^2 m_{Z'}^3}. \quad (\text{A7})$$

Appendix B: Computation of the Chern-Simons coupling

In this section of the appendix we show how to derive an effective Lagrangian from a UV complete model framework, as considered in this work. To achieve this goal, we review computations performed in ref. [50] of potential anomalous diagrams of the theory which involve three external gauge bosons or axions, interacting through a triangular loop of massive fermions. We can classify the possible diagrams in three categories: (1) diagrams without any mass insertions. Such diagrams are linearly divergent and proportional to the usual anomaly trace [143, 144] (see ref. [145] also for an overview). (2) Diagrams involving three gauge bosons with two mass insertions which give a finite result. They are connected to the so-called "CS" interaction (see, for example ref. [50]) and, (3) diagrams involving axions and two gauge bosons with one mass insertion. Just like the former class of diagrams, these diagrams are also finite. We will consider examples where the incoming state for the triangle loop diagrams with heavy fermions is either a gauge boson $A_i^\mu(\vec{k}_3)$ or an axion θ_i while two outgoing states are two gauge fields, denoted as $A_k^\rho(\vec{k}_2)$ and $A_j^\nu(\vec{k}_1)$, respectively. After evaluating these loop diagrams, we also compute the gauge transformations of the effective Lagrangian to ensure an anomaly free setup.

1. Diagrams with two mass insertions : "Chern-Simons" contribution

We initiate our analysis for diagrams having gauge fields in the three external legs and two mass insertions, which is equivalent to have two chirality flips for each diagram. Thus, we can chose one dominant chirality over the remaining two others in the fermionic loop and have three possibilities to place the mass insertions for each dominant chirality. Further, considering the fact that we can contract the external legs of the outgoing gauge fields in two different ways, we end up with twelve diagrams as shown in figure 8.

For a systematic analysis we start with the following Lagrangian:

$$\mathcal{L} \supset \sum_{a=i,j,k} i\bar{F}\partial_\mu\gamma^\mu F - m\bar{F}F - Q_L^a\bar{F}_L\gamma_\mu F_L A_a^\mu - Q_R^a\bar{F}_R\gamma_\mu F_R A_a^\mu, \quad (\text{B1})$$

where $F = F_L + F_R$ are the BSM heavy fermions running in the triangle loops with Q_L^a, Q_R^a as the relevant gauge charges associated with A_μ^a field for the left- and right-chiral BSM fermions, respectively.

We can write contributions of the twelve diagrams without contractions on any external legs as

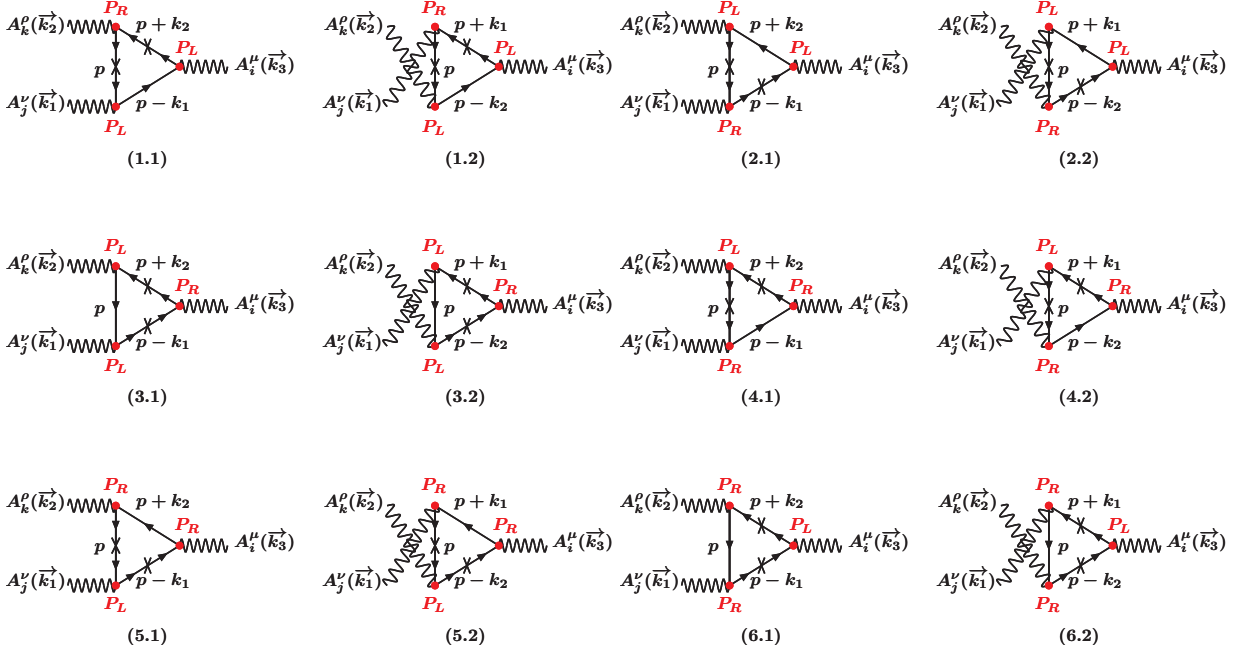


Figure 8. Possible set of diagrams for triangular loops of heavy BSM fermions giving rise to an effective CS interaction. Here ‘ \times ’ denotes a mass insertion and the arrows represent the direction of fermion flow. Directions of the momentum, i.e., p , $p \pm k_1$, $p \mp k_2$, etc. are opposite to the fermion flow.

an integral over the momentum p as:

$$\int \frac{d^4 p}{(2\pi)^4} \Gamma^{\mu\nu\rho}(p, k_1, k_2), \quad (\text{B2})$$

where $\Gamma^{\mu\nu\rho}$, after integrating out heavy fermionic degrees of freedom, can be expanded in the powers of external momentums to achieve the low-energy effective Lagrangian. The expansion goes as:

$$\begin{aligned} \Gamma^{\mu\nu\rho}(p, k_1, k_2) \simeq & \Gamma^{\mu\nu\rho}(p, 0, 0) + \sum_{i=1}^2 k_i^\alpha \left(\frac{\partial \Gamma^{\mu\nu\rho}(p, k_1, k_2)}{\partial k_i^\alpha} \right) \Big|_{k_i=0} \\ & + \frac{1}{2!} \sum_{i,j=1}^2 k_i^\alpha k_j^\beta \left(\frac{\partial^2 \Gamma^{\mu\nu\rho}(p, k_1, k_2)}{\partial k_i^\alpha \partial k_j^\beta} \right) \Big|_{k_{i,j}=0} + \mathcal{O}(k_{i,j}^3). \end{aligned} \quad (\text{B3})$$

Now from figure 8 it is apparent that $\Gamma^{\mu\nu\rho}(p, k_1, k_2)$ can be decomposed as a product of the two terms, i.e., $\Gamma^{\mu\nu\rho}(p, k_1, k_2) = \mathbf{\Pi} \cdot \mathbf{TR}^{\mu\nu\rho}$ where $\mathbf{TR}^{\mu\nu\rho}$ includes possible couplings and traces over gamma matrices while $\mathbf{\Pi}$ is defined in the following way:

$$\begin{aligned} \mathbf{\Pi} &= \frac{1}{p^2 - m^2} \frac{1}{(p + k_2)^2 - m^2} \frac{1}{(p - k_1)^2 - m^2} \quad \text{for diagrams like x.1 with } x=1,2,\dots,6, \\ \text{and } \mathbf{\Pi} &= \frac{1}{p^2 - m^2} \frac{1}{(p - k_2)^2 - m^2} \frac{1}{(p + k_1)^2 - m^2} \quad \text{for diagrams like x.2 with } x=1,2,\dots,6. \end{aligned} \quad (\text{B4})$$

The trace in the leading term $\Gamma(p, 0, 0)$ (see eq. (B3)) appears to be proportional to odd powers of p for the numerator, which vanishes after $\int d^4 p$ integration. The linear and quadratic terms in

k_i^α can be computed straightforwardly from eq. (B3) as :

$$\begin{aligned}
k_i^\alpha \left(\frac{\partial \Gamma^{\mu\nu\rho}(p, k_1, k_2)}{\partial k_i^\alpha} \right) \Big|_{k_i=0} &= k_i^\alpha \left(\frac{\partial \mathbf{TR}^{\mu\nu\rho}}{\partial k_i^\alpha} \cdot \mathbf{\Pi} \right) \Big|_{k_i=0} + k_i^\alpha \left(\frac{\partial \mathbf{\Pi}}{\partial k_i^\alpha} \cdot \mathbf{TR}^{\mu\nu\rho} \right) \Big|_{k_i=0}, \\
k_i^\alpha k_j^\beta \left(\frac{\partial^2 \Gamma^{\mu\nu\rho}(p, k_1, k_2)}{\partial k_i^\alpha \partial k_j^\beta} \right) \Big|_{k_{i,j}=0} &= k_i^\alpha k_j^\beta \left(\frac{\partial^2 \mathbf{TR}^{\mu\nu\rho}}{\partial k_i^\alpha \partial k_j^\beta} \cdot \mathbf{\Pi} \right) \Big|_{k_{i,j}=0} + k_i^\alpha k_j^\beta \left(\frac{\partial^2 \mathbf{\Pi}}{\partial k_i^\alpha \partial k_j^\beta} \cdot \mathbf{TR}^{\mu\nu\rho} \right) \Big|_{k_{i,j}=0} \\
&\quad + k_i^\alpha k_j^\beta \left(\frac{\partial \mathbf{TR}^{\mu\nu\rho}}{\partial k_i^\alpha} \cdot \frac{\partial \mathbf{\Pi}}{\partial k_j^\beta} \right) \Big|_{k_{i,j}=0} + k_i^\alpha k_j^\beta \left(\frac{\partial \mathbf{TR}^{\mu\nu\rho}}{\partial k_j^\beta} \cdot \frac{\partial \mathbf{\Pi}}{\partial k_i^\alpha} \right) \Big|_{k_{i,j}=0} \quad (\text{B5})
\end{aligned}$$

The contributions from denominators $\mathbf{\Pi}$ are shown in eq. (B4) while trace contributions $\mathbf{TR}^{\mu\nu\rho}$ from the twelve diagrams are:

$$\begin{aligned}
\mathbf{TR}_{1.1}^{\mu\nu\rho} &= Q_L^i Q_L^j Q_R^k \text{Tr}[(\not{p} + m)\gamma^\rho P_R(\not{p} + \not{k}_2 + m)\gamma^\mu P_L(\not{p} - \not{k}_1)\gamma^\nu P_L], \\
\mathbf{TR}_{1.2}^{\mu\nu\rho} &= Q_L^i Q_R^j Q_L^k \text{Tr}[(\not{p} + m)\gamma^\rho P_R(\not{p} + \not{k}_1 + m)\gamma^\mu P_L(\not{p} - \not{k}_2)\gamma^\nu P_L], \\
\mathbf{TR}_{2.1}^{\mu\nu\rho} &= Q_L^i Q_R^j Q_L^k \text{Tr}[(\not{p} + m)\gamma^\rho P_L(\not{p} + \not{k}_2)\gamma^\mu P_L(\not{p} - \not{k}_1 + m)\gamma^\nu P_R], \\
\mathbf{TR}_{2.2}^{\mu\nu\rho} &= Q_L^i Q_L^j Q_R^k \text{Tr}[(\not{p} + m)\gamma^\rho P_L(\not{p} + \not{k}_1)\gamma^\mu P_L(\not{p} - \not{k}_2 + m)\gamma^\nu P_R], \\
\mathbf{TR}_{3.1}^{\mu\nu\rho} &= Q_R^i Q_L^j Q_L^k \text{Tr}[\not{p}\gamma^\rho P_L(\not{p} + \not{k}_2 + m)\gamma^\mu P_R(\not{p} - \not{k}_1 + m)\gamma^\nu P_L], \\
\mathbf{TR}_{3.2}^{\mu\nu\rho} &= Q_R^i Q_L^j Q_L^k \text{Tr}[\not{p}\gamma^\rho P_L(\not{p} + \not{k}_1 + m)\gamma^\mu P_R(\not{p} - \not{k}_2 + m)\gamma^\nu P_L], \\
\mathbf{TR}_{4.1}^{\mu\nu\rho} &= Q_R^i Q_R^j Q_L^k \text{Tr}[(\not{p} + m)\gamma^\rho P_L(\not{p} + \not{k}_2 + m)\gamma^\mu P_R(\not{p} - \not{k}_1)\gamma^\nu P_R], \\
\mathbf{TR}_{4.2}^{\mu\nu\rho} &= Q_R^i Q_L^j Q_R^k \text{Tr}[(\not{p} + m)\gamma^\rho P_L(\not{p} + \not{k}_1 + m)\gamma^\mu P_R(\not{p} - \not{k}_2)\gamma^\nu P_R], \\
\mathbf{TR}_{5.1}^{\mu\nu\rho} &= Q_R^i Q_L^j Q_R^k \text{Tr}[(\not{p} + m)\gamma^\rho P_R(\not{p} + \not{k}_2)\gamma^\mu P_R(\not{p} - \not{k}_1 + m)\gamma^\nu P_L], \\
\mathbf{TR}_{5.2}^{\mu\nu\rho} &= Q_R^i Q_R^j Q_L^k \text{Tr}[(\not{p} + m)\gamma^\rho P_R(\not{p} + \not{k}_1)\gamma^\mu P_R(\not{p} - \not{k}_2 + m)\gamma^\nu P_L], \\
\mathbf{TR}_{6.1}^{\mu\nu\rho} &= Q_L^i Q_R^j Q_R^k \text{Tr}[\not{p}\gamma^\rho P_R(\not{p} + \not{k}_2 + m)\gamma^\mu P_L(\not{p} - \not{k}_1 + m)\gamma^\nu P_R], \\
\mathbf{TR}_{6.2}^{\mu\nu\rho} &= Q_L^i Q_R^j Q_R^k \text{Tr}[\not{p}\gamma^\rho P_R(\not{p} + \not{k}_1 + m)\gamma^\mu P_L(\not{p} - \not{k}_2 + m)\gamma^\nu P_R], \quad (\text{B6})
\end{aligned}$$

where mass insertions are properly taken into account.

One can use eq. (B5) to extract contributions from the twelve diagrams shown in figure 8. For example, the contribution proportional to $Q_L^i Q_L^j Q_R^k$ involving diagrams (1.1) and (2.2), in the linear terms of eq. (B5), gives:

$$\begin{aligned}
\int \frac{d^4 p}{(2\pi)^4} \left(\Gamma_{(1.1)}^{\mu\nu\rho} + \Gamma_{(2.2)}^{\mu\nu\rho} \right) &= 8im^2 Q_L^i Q_L^j Q_R^k \epsilon^{\mu\nu\rho\sigma} \int \frac{d^4 p}{(2\pi)^4} \left[\frac{(k_2 - k_1)_\sigma}{4} \frac{p^2}{(p^2 - m^2)^4} + \frac{k_{1\sigma}}{2(p^2 - m^2)^3} \right], \\
&= Q_L^i Q_L^j Q_R^k \epsilon^{\mu\nu\rho\sigma} \frac{1}{24\pi^2} (k_3 + k_1)_\sigma, \quad (\text{B7})
\end{aligned}$$

where we used the known expressions for different momentum integrals over p (see ref. [146] for example) and $k_1 + k_2 = k_3$. In a similar way the contributions from all the twelve diagrams of figure 8 can be grouped as shown in table B 1.

Diagrams	Contribution to $\Gamma^{\mu\nu\rho}$
(1.1)+(2.2)	$Q_L^i Q_L^j Q_R^k \epsilon^{\mu\nu\rho\sigma} (k_3 + k_1)_\sigma / (24\pi^2)$
(2.1)+(1.2)	$-Q_L^i Q_R^j Q_L^k \epsilon^{\mu\nu\rho\sigma} (k_3 + k_2)_\sigma / (24\pi^2)$
(3.1)+(3.2)	$Q_R^i Q_L^j Q_L^k \epsilon^{\mu\nu\rho\sigma} (k_2 - k_1)_\sigma / (24\pi^2)$
(4.1)+(5.2)	$-Q_R^i Q_R^j Q_L^k \epsilon^{\mu\nu\rho\sigma} (k_3 + k_1)_\sigma / (24\pi^2)$
(5.1)+(4.2)	$Q_R^i Q_L^j Q_R^k \epsilon^{\mu\nu\rho\sigma} (k_3 + k_2)_\sigma / (24\pi^2)$
(6.1)+(6.2)	$Q_L^i Q_R^j Q_R^k \epsilon^{\mu\nu\rho\sigma} (k_1 - k_2)_\sigma / (24\pi^2)$

Table II. Resultant contributions of the twelve diagrams of figure 8, clubbed according to the same pre-factor.

From table B1, one can factorize the sum of all contributions proportional to the external momentum k_3 as:

$$\begin{aligned}
\int \frac{d^4 p}{(2\pi)^4} \Gamma^{\mu\nu\rho} &\supset \frac{1}{24\pi^2} \epsilon^{\mu\nu\rho\sigma} k_{3\sigma} (Q_L^i Q_L^j Q_R^k - Q_L^i Q_R^j Q_L^k - Q_R^i Q_R^j Q_L^k + Q_R^i Q_L^j Q_R^k), \\
&\supset \frac{1}{24\pi^2} \epsilon^{\mu\nu\rho\sigma} k_{3\sigma} (Q_L^i + Q_R^i) (Q_L^j Q_R^k - Q_L^k Q_R^j).
\end{aligned} \tag{B8}$$

The same factorization can be done for k_2 and k_1 to produce the following effective Lagrangian :

$$\mathcal{L}_{\text{CS}}^{\text{eff}} = \frac{1}{96\pi^2} (Q_L^k + Q_R^k) (Q_L^i Q_R^j - Q_L^j Q_R^i) \epsilon_{\mu\nu\rho\sigma} A_i^\mu A_j^\nu F_k^{\rho\sigma}, \tag{B9}$$

where summation over all the possible combinations of the gauge fields is implied.

2. Diagrams with axions

The diagrams involving an axion field θ_i include only one mass insertion since vertices with two fermionic legs and an axion field flips the chirality, as evidenced from the following Lagrangian:

$$\mathcal{L}^{\text{axion}} = -iy_F \theta_i \bar{F}_L F_R + \text{h.c.} - m \bar{F} F = -iy_F \theta_i \bar{F} \gamma_5 F - m \bar{F} F, \tag{B10}$$

where y_F is the associated Yukawa coupling. For the chosen Lagrangian we have three possible ways to place a mass insertion on the fermionic propagators and two different ways to connect the external lines with the vertices, giving a total of six diagrams as shown in figure 9.

Once again, like the CS case (see eq. (B2)), we can write the sum over the six diagrams without contractions on the external legs as an integral over the momentum p as:

$$\int \frac{d^4 p}{(2\pi)^4} \Gamma^{\nu\rho}(p, k_1, k_2), \tag{B11}$$

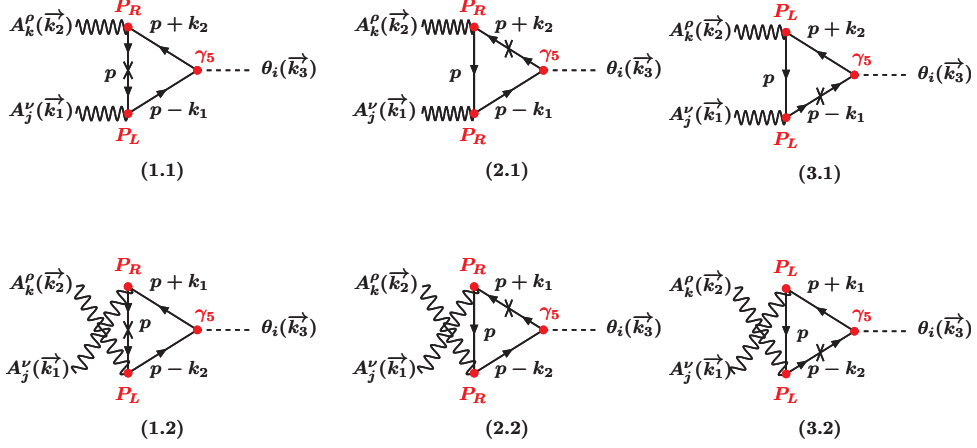


Figure 9. Possible set of diagrams for triangular loops of heavy BSM fermions with an external axion field. Here ‘ \times ’ denotes a mass insertion and the arrows represent the direction of fermion flow. Directions of the momentum, i.e., p , $p \pm k_1$, $p \mp k_2$, etc. are opposite to the fermion flow.

where $\Gamma^{\nu\rho}(p, k_1, k_2)$ is decomposed as $\mathbf{\Pi} \cdot \mathbf{TR}^{\nu\rho}$ with $\mathbf{\Pi}$ as already defined in eq. (B4) and the trace factors $\mathbf{TR}^{\nu\rho}$ written as:

$$\begin{aligned}
\mathbf{TR}_{1.1}^{\nu\rho} &= y_F Q_L^j Q_R^k \text{Tr}[\gamma_5(\not{p} - \not{k}_1)\gamma^\nu P_L(\not{p} + m)\gamma^\rho P_R(\not{p} + \not{k}_2)], \\
\mathbf{TR}_{1.2}^{\nu\rho} &= y_F Q_R^j Q_L^k \text{Tr}[\gamma_5(\not{p} - \not{k}_2)\gamma^\rho P_L(\not{p} + m)\gamma^\nu P_R(\not{p} + \not{k}_1)], \\
\mathbf{TR}_{2.1}^{\nu\rho} &= y_F Q_R^j Q_R^k \text{Tr}[\gamma_5(\not{p} - \not{k}_1)\gamma^\nu P_R\not{p}\gamma^\rho P_R(\not{p} + \not{k}_2 + m)], \\
\mathbf{TR}_{2.2}^{\nu\rho} &= y_F Q_R^j Q_R^k \text{Tr}[\gamma_5(\not{p} - \not{k}_2)\gamma^\rho P_R\not{p}\gamma^\nu P_R(\not{p} + \not{k}_1 + m)], \\
\mathbf{TR}_{3.1}^{\nu\rho} &= y_F Q_L^j Q_L^k \text{Tr}[\gamma_5(\not{p} - \not{k}_1 + m)\gamma^\nu P_L\not{p}\gamma^\rho P_L(\not{p} + \not{k}_2)], \\
\mathbf{TR}_{3.2}^{\nu\rho} &= y_F Q_L^j Q_L^k \text{Tr}[\gamma_5(\not{p} - \not{k}_2 + m)\gamma^\rho P_L\not{p}\gamma^\nu P_L(\not{p} + \not{k}_1)],
\end{aligned} \tag{B12}$$

with proper mass insertion.

Now if we consider expansion of $\Gamma^{\nu\rho}(p, k_1, k_2)$ in powers of the external momenta k_1, k_2 , just like the already studied CS scenario, the zeroth and linear order terms of the expansion vanish. This happens as the former is proportional to k_i while the latter yields contributions $\propto p$ and thus, disappears after performing $\int d^4p$ over an odd function. The leading contribution thus, comes from the second order. Considering a CP invariant UV complete theory, we keep only the CP-odd contribution in $\Gamma^{\nu\rho}(p, k_1, k_2)$ since axions are CP-odd fields. With this approach one can compute the detail expressions for all the six diagrams of figure 9, for example, for the diagram (3.1) one

gets:

$$\begin{aligned} \int \frac{d^4 p}{(2\pi)^4} \Gamma_{(3.1)}^{\nu\rho}(p, k_1, k_2) &= im y_F Q_L^j Q_L^k \epsilon^{\mu\nu\rho\sigma} k_{1\rho} k_{2\sigma} \int \frac{d^4 p}{(2\pi)^4} \frac{p^2}{(p^2 - m^2)^4}, \\ &= \frac{1}{v_i} \frac{Q_L^j Q_L^k}{48\pi^2} \epsilon^{\nu\rho\alpha\beta} k_{1\alpha} k_{2\beta}, \end{aligned} \quad (\text{B13})$$

where in the last step we have used the known momentum integral as of ref. [146] as well as $m = y_F v_i$ with v_i being the VEV of the scalar field giving masses to the BSM fermions F and the gauge field A_i^μ . In a similar way the contributions from all the six diagrams of figure 9 can be evaluated as tabulated in table B 2.

Diagrams	Contribution to $\Gamma^{\nu\rho}$
(1.1)	$Q_L^j Q_R^k \epsilon^{\nu\rho\alpha\beta} k_{1\alpha} k_{2\beta} / (48\pi^2 v_i)$
(2.1)	$Q_R^j Q_R^k \epsilon^{\nu\rho\alpha\beta} k_{1\alpha} k_{2\beta} / (48\pi^2 v_i)$
(3.1)	$Q_L^j Q_L^k \epsilon^{\nu\rho\alpha\beta} k_{1\alpha} k_{2\beta} / (48\pi^2 v_i)$
(1.2)	$Q_R^j Q_L^k \epsilon^{\nu\rho\alpha\beta} k_{1\alpha} k_{2\beta} / (48\pi^2 v_i)$
(2.2)	$Q_R^j Q_R^k \epsilon^{\nu\rho\alpha\beta} k_{1\alpha} k_{2\beta} / (48\pi^2 v_i)$
(3.2)	$Q_L^j Q_L^k \epsilon^{\nu\rho\alpha\beta} k_{1\alpha} k_{2\beta} / (48\pi^2 v_i)$

Table III. Final contributions of the six diagrams of figure 9.

Summing all the six contributions from table B 2 yields :

$$\int \frac{d^4 p}{(2\pi)^4} \Gamma^{\nu\rho} = \frac{1}{v_i} \frac{1}{48\pi^2} \epsilon^{\nu\rho\alpha\beta} k_{1\alpha} k_{2\beta} [2(Q_L^j Q_L^k + Q_R^j Q_R^k) + Q_R^j Q_L^k + Q_L^j Q_R^k],$$

which finally produce the following effective Lagrangian:

$$\mathcal{L}_{\text{axion}}^{\text{eff}} = \frac{1}{192\pi^2} [2(Q_L^j Q_L^k + Q_R^j Q_R^k) + Q_R^j Q_L^k + Q_L^j Q_R^k] \epsilon_{\mu\nu\rho\sigma} \frac{\theta_i}{v_i} F_j^{\mu\nu} F_k^{\rho\sigma}, \quad (\text{B14})$$

where, once again summation over all the possible combinations of the gauge fields is implied.

3. Anomaly cancellation

In the last two subsections we discussed about the three different anomalous contributions, namely, (1) diagrams without any chirality flip which are linearly divergent and giving contributions proportional to the anomaly traces. (2) Diagrams with one chirality flip involving an axion field that are finite and, (3) the so-called "CS" contributions which are finite and invoke two chirality flips. In this subsection we show that gauge transformation of the effective CS and axion Lagrangians (see

eq. (B9) and eq. (B14)) is proportional to the “usual” anomaly trace. Hence, a vanishing anomaly trace, with appropriate distribution of the charges of BSM fermions, assures an anomaly free theory construction. Given the following gauge transformations of an axion field θ_i and a gauge field A_i^μ :

$$\theta_i \rightarrow \theta_i + v_i(Q_L^i - Q_R^i)\alpha_i, \quad A_i^\mu \rightarrow A_i^\mu + \partial^\mu \alpha_i, \quad (\text{B15})$$

where α_i is the parameter of gauge transformation, the variation of the effective CS Lagrangian (see eq. (B9)) becomes:

$$\delta\mathcal{L}^{\text{CS}} = -\frac{1}{192\pi^2} \left[(Q_L^k + Q_R^k)(Q_L^i Q_R^j - Q_L^j Q_R^i) + (Q_L^j + Q_R^j)(Q_L^i Q_R^k - Q_L^k Q_R^i) \right] \epsilon_{\mu\nu\rho\sigma} \alpha_i F_j^{\mu\nu} F_k^{\rho\sigma}, \quad (\text{B16})$$

where we have used the advantages of integrating by parts as well as Bianchi identity and included all possible combinations of the i, j, k indices. The change in effective axion Lagrangian (see eq. (B14)) is given by:

$$\delta\mathcal{L}^{\text{axion}} = \frac{1}{192\pi^2} [2(Q_L^j Q_L^k + Q_R^j Q_R^k) + Q_R^j Q_L^k + Q_L^j Q_R^k] (Q_L^i - Q_R^i) \alpha_i \epsilon_{\mu\nu\rho\sigma} F_j^{\mu\nu} F_k^{\rho\sigma}. \quad (\text{B17})$$

Combining eq. (B16) and eq. (B17) the resultant variation, given the transformations of eq. (B15), is written as:

$$\delta\mathcal{L} = \delta\mathcal{L}^{\text{axion}} + \delta\mathcal{L}^{\text{CS}} = \frac{1}{96\pi^2} \alpha_i \left[Q_L^i Q_L^j Q_L^k - Q_R^i Q_R^j Q_R^k \right] \epsilon_{\mu\nu\rho\sigma} F_j^{\mu\nu} F_k^{\rho\sigma}. \quad (\text{B18})$$

It is now apparent from eq. (B18) that gauge transformation of the total Lagrangian, i.e., axion and CS Lagrangians is proportional to the “usual” anomaly trace $Q_L^i Q_L^j Q_L^k - Q_R^i Q_R^j Q_R^k$. Hence, with proper choice of the charges for the heavy fermions one can ensure an anomaly free theory setup where the anomaly trace $Q_L^i Q_L^j Q_L^k - Q_R^i Q_R^j Q_R^k$ vanishes for all i, j, k . Further, when this anomaly trace disappears with proper choice of $Q_L^i, Q_R^i, Q_L^j, Q_R^j, Q_L^k$ and Q_R^k , the combination of the axion and CS effective Lagrangians (i.e., eq. (B9) + eq. (B14)) can be embedded into a dimension-six operator as:

$$\epsilon_{\mu\nu\rho\sigma} D^\mu \theta_i D^\nu \theta_j F_k^{\rho\sigma}, \quad (\text{B19})$$

where D^μ, D^ν are co-variant derivatives for axion fields θ_i, θ_j , respectively. One can always consider the case of unitary gauge when the axion Lagrangian (see eq. (B14)) vanishes and the total Lagrangian is simply the CS one, as given by eq. (B9). This is the scenario which we studied in this work. Recasting eq. (B9) for the specific case of $U(1)_X \times U(1)_V$, as considered in this work, one can generate

$$\mathcal{L} = \mathcal{L}_{\text{CS}}^{\text{eff}} = \frac{1}{48\pi^2} (Q_L^X + Q_R^X)(Q_L^X Q_R^V - Q_L^V Q_R^X) \epsilon_{\mu\nu\rho\sigma} X^\mu \tilde{V}^\nu X^{\rho\sigma} \equiv \alpha_{\text{CS}} \epsilon_{\mu\nu\rho\sigma} X^\mu \tilde{V}^\nu X^{\rho\sigma}, \quad (\text{B20})$$

where terms $\propto \epsilon_{\mu\nu\rho\sigma} \tilde{V}^\mu X^\nu \tilde{V}^{\rho\sigma}$ is effaced with suitable choice of associated charges and the parameter α_{CS} is given by

$$\alpha_{\text{CS}} \equiv \frac{1}{48\pi^2} (Q_L^X + Q_R^X)(Q_L^X Q_R^V - Q_L^V Q_R^X), \quad (\text{B21})$$

which we have already used to derive eq. 44 for the charges given in table I.

-
- [1] G. Bertone, D. Hooper, and J. Silk, *Phys. Rept.* **405**, 279 (2005), arXiv:hep-ph/0404175 [hep-ph].
 - [2] J. Silk *et al.*, *Particle Dark Matter: Observations, Models and Searches*, edited by G. Bertone (Cambridge Univ. Press, Cambridge, 2010).
 - [3] S. Profumo, in *Proceedings, Theoretical Advanced Study Institute in Elementary Particle Physics: Searching for New Physics at Small and Large Scales (TASI 2012): Boulder, Colorado, June 4-29, 2012* (2013) pp. 143–189, arXiv:1301.0952 [hep-ph].
 - [4] L. E. Strigari, *Phys. Rept.* **531**, 1 (2013), arXiv:1211.7090 [astro-ph.CO].
 - [5] G. Bertone and D. Hooper, Submitted to: *Rev. Mod. Phys.* (2016), arXiv:1605.04909 [astro-ph.CO].
 - [6] P. A. R. Ade *et al.* (Planck), *Astron. Astrophys.* **594**, A13 (2016), arXiv:1502.01589 [astro-ph.CO].
 - [7] J. Angle *et al.* (XENON), *Phys. Rev. Lett.* **100**, 021303 (2008), arXiv:0706.0039 [astro-ph].
 - [8] J. Angle *et al.*, *Phys. Rev. Lett.* **101**, 091301 (2008), arXiv:0805.2939 [astro-ph].
 - [9] R. Essig, A. Manalaysay, J. Mardon, P. Sorensen, and T. Volansky, *Phys. Rev. Lett.* **109**, 021301 (2012), arXiv:1206.2644 [astro-ph.CO].
 - [10] E. Aprile *et al.* (XENON100), *Phys. Rev. Lett.* **111**, 021301 (2013), arXiv:1301.6620 [astro-ph.CO].
 - [11] E. Aprile *et al.* (XENON100), *Phys. Rev.* **D90**, 062009 (2014), [Erratum: *Phys. Rev.* **D95** (2017) 029904], arXiv:1404.1455 [astro-ph.CO].
 - [12] D. S. Akerib *et al.* (LUX), *Phys. Rev. Lett.* **116**, 161301 (2016), arXiv:1512.03506 [astro-ph.CO].
 - [13] P. Agnes *et al.* (DarkSide), *Phys. Rev.* **D93**, 081101 (2016), [Addendum: *Phys. Rev.* **D95** (2017) 069901], arXiv:1510.00702 [astro-ph.CO].
 - [14] C. Amole *et al.* (PICO), *Phys. Rev.* **D93**, 052014 (2016), arXiv:1510.07754 [hep-ex].
 - [15] G. Angloher *et al.* (CRESSST), *Eur. Phys. J.* **C76**, 25 (2016), arXiv:1509.01515 [astro-ph.CO].
 - [16] L. Hehn *et al.* (EDELWEISS), *Eur. Phys. J.* **C76**, 548 (2016), arXiv:1607.03367 [astro-ph.CO].
 - [17] D. S. Akerib *et al.* (LUX), *Phys. Rev. Lett.* **116**, 161302 (2016), arXiv:1602.03489 [hep-ex].
 - [18] E. Aprile *et al.* (XENON100), *Phys. Rev.* **D94**, 122001 (2016), arXiv:1609.06154 [astro-ph.CO].
 - [19] C. Amole *et al.* (PICO), *Phys. Rev.* **D93**, 061101 (2016), arXiv:1601.03729 [astro-ph.CO].
 - [20] C. Amole *et al.* (PICO), (2017), arXiv:1702.07666 [astro-ph.CO].
 - [21] T. Hambye, *JHEP* **01**, 028 (2009), arXiv:0811.0172 [hep-ph].
 - [22] J. L. Diaz-Cruz and E. Ma, *Phys. Lett.* **B695**, 264 (2011), arXiv:1007.2631 [hep-ph].

- [23] J. K. Mizukoshi, C. A. de S. Pires, F. S. Queiroz, and P. S. Rodrigues da Silva, *Phys. Rev.* **D83**, 065024 (2011), arXiv:1010.4097 [hep-ph].
- [24] S. Bhattacharya, J. L. Diaz-Cruz, E. Ma, and D. Wegman, *Phys. Rev.* **D85**, 055008 (2012), arXiv:1107.2093 [hep-ph].
- [25] Y. Farzan and A. R. Akbarieh, *JCAP* **1210**, 026 (2012), arXiv:1207.4272 [hep-ph].
- [26] S. Baek, P. Ko, W.-I. Park, and E. Senaha, *JHEP* **05**, 036 (2013), arXiv:1212.2131 [hep-ph].
- [27] C. D. Carone and R. Ramos, *Phys. Rev.* **D88**, 055020 (2013), arXiv:1307.8428 [hep-ph].
- [28] C.-R. Chen, Y.-K. Chu, and H.-C. Tsai, *Phys. Lett.* **B741**, 205 (2015), arXiv:1410.0918 [hep-ph].
- [29] P. W. Graham, J. Mardon, and S. Rajendran, *Phys. Rev.* **D93**, 103520 (2016), arXiv:1504.02102 [hep-ph].
- [30] C.-H. Chen and T. Nomura, *Phys. Rev.* **D93**, 074019 (2016), arXiv:1507.00886 [hep-ph].
- [31] A. DiFranzo, P. J. Fox, and T. M. P. Tait, *JHEP* **04**, 135 (2016), arXiv:1512.06853 [hep-ph].
- [32] G. Bambhaniya, J. Kumar, D. Marfatia, A. C. Nayak, and G. Tomar, *Phys. Lett.* **B766**, 177 (2017), arXiv:1609.05369 [hep-ph].
- [33] B. Barman, S. Bhattacharya, S. K. Patra, and J. Chakraborty, (2017), arXiv:1704.04945 [hep-ph].
- [34] G. Arcadi, M. Dutra, P. Ghosh, M. Lindner, Y. Mambrini, M. Pierre, S. Profumo, and F. S. Queiroz, (2017), arXiv:1703.07364 [hep-ph].
- [35] M. Escudero, A. Berlin, D. Hooper, and M.-X. Lin, *JCAP* **1612**, 029 (2016), arXiv:1609.09079 [hep-ph].
- [36] J. Abdallah *et al.*, *Phys. Dark Univ.* **9-10**, 8 (2015), arXiv:1506.03116 [hep-ph].
- [37] F. Kahlhoefer, K. Schmidt-Hoberg, T. Schwetz, and S. Vogl, *JHEP* **02**, 016 (2016), arXiv:1510.02110 [hep-ph].
- [38] C. Englert, M. McCullough, and M. Spannowsky, *Phys. Dark Univ.* **14**, 48 (2016), arXiv:1604.07975 [hep-ph].
- [39] N. F. Bell, Y. Cai, and R. K. Leane, *JCAP* **1701**, 039 (2017), arXiv:1610.03063 [hep-ph].
- [40] D. Goncalves, P. A. N. Machado, and J. M. No, (2016), arXiv:1611.04593 [hep-ph].
- [41] N. F. Bell, G. Busoni, and I. W. Sanderson, *JCAP* **1703**, 015 (2017), arXiv:1612.03475 [hep-ph].
- [42] B. Holdom, *Phys. Lett.* **B166**, 196 (1986).
- [43] F. del Aguila, G. D. Coughlan, and M. Quiros, *Nucl. Phys.* **B307**, 633 (1988), [Erratum: *Nucl. Phys.* **B312** (1989) 751].
- [44] F. del Aguila, M. Masip, and M. Perez-Victoria, *Nucl. Phys.* **B456**, 531 (1995), arXiv:hep-ph/9507455 [hep-ph].
- [45] R. Foot and X.-G. He, *Phys. Lett.* **B267**, 509 (1991).
- [46] E. Dudas, Y. Mambrini, S. Pokorski, and A. Romagnoni, *JHEP* **08**, 014 (2009), arXiv:0904.1745 [hep-ph].
- [47] Y. Mambrini, *JCAP* **0912**, 005 (2009), arXiv:0907.2918 [hep-ph].
- [48] E. Dudas, Y. Mambrini, S. Pokorski, and A. Romagnoni, *JHEP* **10**, 123 (2012), arXiv:1205.1520

- [hep-ph].
- [49] E. Dudas, L. Heurtier, Y. Mambrini, and B. Zaldivar, *JHEP* **11**, 083 (2013), arXiv:1307.0005 [hep-ph].
- [50] P. Anastasopoulos, M. Bianchi, E. Dudas, and E. Kiritsis, *JHEP* **11**, 057 (2006), arXiv:hep-th/0605225 [hep-th].
- [51] G. Arcadi, M. Lindner, Y. Mambrini, M. Pierre, and F. S. Queiroz, (2017), arXiv:1704.02328 [hep-ph].
- [52] M. B. Green and J. H. Schwarz, *Phys. Lett.* **B149**, 117 (1984).
- [53] M. B. Green and J. H. Schwarz, *Phys. Lett.* **B151**, 21 (1985).
- [54] G. Arcadi, Y. Mambrini, M. H. G. Tytgat, and B. Zaldivar, *JHEP* **03**, 134 (2014), arXiv:1401.0221 [hep-ph].
- [55] S. Profumo and F. S. Queiroz, *Eur. Phys. J.* **C74**, 2960 (2014), arXiv:1307.7802 [hep-ph].
- [56] J. M. Cline, G. Dupuis, Z. Liu, and W. Xue, *JHEP* **08**, 131 (2014), arXiv:1405.7691 [hep-ph].
- [57] O. Lebedev and Y. Mambrini, *Phys. Lett.* **B734**, 350 (2014), arXiv:1403.4837 [hep-ph].
- [58] A. De Simone, G. F. Giudice, and A. Strumia, *JHEP* **06**, 081 (2014), arXiv:1402.6287 [hep-ph].
- [59] W.-Z. Feng, G. Shiu, P. Soler, and F. Ye, *Phys. Rev. Lett.* **113**, 061802 (2014), arXiv:1401.5880 [hep-ph].
- [60] O. Buchmueller, M. J. Dolan, S. A. Malik, and C. McCabe, *JHEP* **01**, 037 (2015), arXiv:1407.8257 [hep-ph].
- [61] M. Fairbairn and J. Heal, *Phys. Rev.* **D90**, 115019 (2014), arXiv:1406.3288 [hep-ph].
- [62] B. Allanach, F. S. Queiroz, A. Strumia, and S. Sun, *Phys. Rev.* **D93**, 055045 (2016), arXiv:1511.07447 [hep-ph].
- [63] A. Alves, A. Berlin, S. Profumo, and F. S. Queiroz, *JHEP* **10**, 076 (2015), arXiv:1506.06767 [hep-ph].
- [64] A. Alves, A. Berlin, S. Profumo, and F. S. Queiroz, *Phys. Rev.* **D92**, 083004 (2015), arXiv:1501.03490 [hep-ph].
- [65] T. Marrodán Undagoitia and L. Rauch, *J. Phys.* **G43**, 013001 (2016), arXiv:1509.08767 [physics.ins-det].
- [66] O. Ducu, L. Heurtier, and J. Maurer, *JHEP* **03**, 006 (2016), arXiv:1509.05615 [hep-ph].
- [67] M. Fairbairn, J. Heal, F. Kahlhoefer, and P. Tunney, *JHEP* **09**, 018 (2016), arXiv:1605.07940 [hep-ph].
- [68] M. Klasen, F. Lyonnet, and F. S. Queiroz, (2016), arXiv:1607.06468 [hep-ph].
- [69] A. Alves, G. Arcadi, Y. Mambrini, S. Profumo, and F. S. Queiroz, (2016), arXiv:1612.07282 [hep-ph].
- [70] T. Jacques, A. Katz, E. Morgante, D. Racco, M. Rameez, and A. Riotto, *JHEP* **10**, 071 (2016), arXiv:1605.06513 [hep-ph].
- [71] W. Altmannshofer, S. Gori, S. Profumo, and F. S. Queiroz, *JHEP* **12**, 106 (2016), arXiv:1609.04026 [hep-ph].
- [72] N. Okada and S. Okada, *Phys. Rev.* **D95**, 035025 (2017), arXiv:1611.02672 [hep-ph].
- [73] A. Alves, G. Arcadi, P. V. Dong, L. Duarte, F. S. Queiroz, and J. W. F. Valle, (2016), arXiv:1612.04383 [hep-ph].
- [74] K. S. Babu, C. F. Kolda, and J. March-Russell, *Phys. Rev.* **D57**, 6788 (1998), arXiv:hep-ph/9710441

- [hep-ph].
- [75] E. J. Chun, J.-C. Park, and S. Scopel, *JHEP* **02**, 100 (2011), arXiv:1011.3300 [hep-ph].
- [76] Y. Mambrini, *JCAP* **1009**, 022 (2010), arXiv:1006.3318 [hep-ph].
- [77] Y. Mambrini, *JCAP* **1107**, 009 (2011), arXiv:1104.4799 [hep-ph].
- [78] C. Patrignani *et al.* (Particle Data Group), *Chin. Phys.* **C40**, 100001 (2016).
- [79] J. Kumar and J. D. Wells, *Phys. Rev.* **D74**, 115017 (2006), arXiv:hep-ph/0606183 [hep-ph].
- [80] M. Aaboud *et al.* (ATLAS), *Phys. Lett.* **B761**, 372 (2016), arXiv:1607.03669 [hep-ex].
- [81] V. Khachatryan *et al.* (CMS), *Phys. Lett.* **B768**, 57 (2017), arXiv:1609.05391 [hep-ex].
- [82] ATLAS-CONF-2017-027 (ATLAS), (2017), aTLAS-CONF-2017-027.
- [83] V. Khachatryan *et al.* (CMS), *Phys. Rev. Lett.* **116**, 071801 (2016), arXiv:1512.01224 [hep-ex].
- [84] G. Aad *et al.* (ATLAS), *Phys. Lett.* **B754**, 302 (2016), arXiv:1512.01530 [hep-ex].
- [85] A. M. Sirunyan *et al.* (CMS), *Phys. Lett. B* (2016), 10.1016/j.physletb.2017.02.012, arXiv:1611.03568 [hep-ex].
- [86] M. Aaboud *et al.* (ATLAS), (2017), arXiv:1703.09127 [hep-ex].
- [87] A. M. Sirunyan *et al.* (CMS), (2017), arXiv:1703.01651 [hep-ex].
- [88] M. Aaboud *et al.* (ATLAS), *Phys. Lett.* **B763**, 251 (2016), arXiv:1608.02372 [hep-ex].
- [89] CMS-PAS-EXO-16-038 (CMS), (2016).
- [90] M. Aaboud *et al.* (ATLAS), *JHEP* **06**, 059 (2016), arXiv:1604.01306 [hep-ex].
- [91] CMS-PAS-EXO-16-039 (CMS), (2016).
- [92] M. Aaboud *et al.* (ATLAS), (2017), arXiv:1704.03848 [hep-ex].
- [93] ATLAS-CONF-2017-024 (ATLAS), (2017).
- [94] ATLAS-CONF-2017-028 (ATLAS), (2017).
- [95] A. M. Sirunyan *et al.* (CMS), (2017), arXiv:1703.05236 [hep-ex].
- [96] P. Gondolo and G. Gelmini, *Nucl. Phys.* **B360**, 145 (1991).
- [97] G. Jungman, M. Kamionkowski, and K. Griest, *Phys. Rept.* **267**, 195 (1996), arXiv:hep-ph/9506380 [hep-ph].
- [98] K. Griest and D. Seckel, *Phys. Rev.* **D43**, 3191 (1991).
- [99] G. Bélanger, F. Boudjema, A. Pukhov, and A. Semenov, *Comput. Phys. Commun.* **176**, 367 (2007), arXiv:hep-ph/0607059 [hep-ph].
- [100] G. Bélanger, F. Boudjema, A. Pukhov, and A. Semenov, *Comput. Phys. Commun.* **180**, 747 (2009), arXiv:0803.2360 [hep-ph].
- [101] G. Bélanger, F. Boudjema, A. Pukhov, and A. Semenov, *Comput. Phys. Commun.* **185**, 960 (2014), arXiv:1305.0237 [hep-ph].
- [102] N. D. Christensen and C. Duhr, *Comput. Phys. Commun.* **180**, 1614 (2009), arXiv:0806.4194 [hep-ph].
- [103] A. Alloul, N. D. Christensen, C. Degrande, C. Duhr, and B. Fuks, *Comput. Phys. Commun.* **185**, 2250 (2014), arXiv:1310.1921 [hep-ph].
- [104] M. Ackermann *et al.* (Fermi-LAT), *Phys. Rev. Lett.* **115**, 231301 (2015), arXiv:1503.02641 [astro-

- ph.HE].
- [105] A. Abramowski *et al.* (H.E.S.S.), Phys. Rev. Lett. **106**, 161301 (2011), arXiv:1103.3266 [astro-ph.HE].
 - [106] M. L. Ahnen *et al.* (Fermi-LAT, MAGIC), JCAP **1602**, 039 (2016), arXiv:1601.06590 [astro-ph.HE].
 - [107] H. Abdallah *et al.* (H.E.S.S.), Phys. Rev. Lett. **117**, 111301 (2016), arXiv:1607.08142 [astro-ph.HE].
 - [108] M. Doro *et al.* (CTA Consortium), Astropart. Phys. **43**, 189 (2013), arXiv:1208.5356 [astro-ph.IM].
 - [109] M. Pierre, J. M. Siegal-Gaskins, and P. Scott, JCAP **1406**, 024 (2014), [Erratum: JCAP **1410** (2014) E01], arXiv:1401.7330 [astro-ph.HE].
 - [110] M. Wood, J. Buckley, S. Digel, S. Funk, D. Nieto, and M. A. Sanchez-Conde, in *Proceedings, Community Summer Study 2013: Snowmass on the Mississippi (CSS2013): Minneapolis, MN, USA, July 29-August 6, 2013* (2013) arXiv:1305.0302 [astro-ph.HE].
 - [111] H. Silverwood, C. Weniger, P. Scott, and G. Bertone, JCAP **1503**, 055 (2015), arXiv:1408.4131 [astro-ph.HE].
 - [112] V. Lefranc, E. Moulin, P. Panci, and J. Silk, Phys. Rev. **D91**, 122003 (2015), arXiv:1502.05064 [astro-ph.HE].
 - [113] V. Lefranc, G. A. Mamon, and P. Panci, JCAP **1609**, 021 (2016), arXiv:1605.02793 [astro-ph.HE].
 - [114] D. S. Akerib *et al.* (LUX), Phys. Rev. Lett. **118**, 021303 (2017), arXiv:1608.07648 [astro-ph.CO].
 - [115] A. Tan *et al.* (PandaX-II), Phys. Rev. Lett. **117**, 121303 (2016), arXiv:1607.07400 [hep-ex].
 - [116] C. Fu *et al.* (PandaX-II), Phys. Rev. Lett. **118**, 071301 (2017), arXiv:1611.06553 [hep-ex].
 - [117] K. Griest and M. Kamionkowski, Phys. Rev. Lett. **64**, 615 (1990).
 - [118] J. F. Beacom, N. F. Bell, and G. D. Mack, Phys. Rev. Lett. **99**, 231301 (2007), arXiv:astro-ph/0608090 [astro-ph].
 - [119] J. Alwall, R. Frederix, S. Frixione, V. Hirschi, F. Maltoni, O. Mattelaer, H. S. Shao, T. Stelzer, P. Torrielli, and M. Zaro, JHEP **07**, 079 (2014), arXiv:1405.0301 [hep-ph].
 - [120] T. Sjöstrand, S. Ask, J. R. Christiansen, R. Corke, N. Desai, P. Ilten, S. Mrenna, S. Prestel, C. O. Rasmussen, and P. Z. Skands, Comput. Phys. Commun. **191**, 159 (2015), arXiv:1410.3012 [hep-ph].
 - [121] J. de Favereau, C. Delaere, P. Demin, A. Giammanco, V. Lemaître, A. Mertens, and M. Selvaggi (DELPHES 3), JHEP **02**, 057 (2014), arXiv:1307.6346 [hep-ex].
 - [122] D. Hooper, C. Kelso, and F. S. Queiroz, Astropart. Phys. **46**, 55 (2013), arXiv:1209.3015 [astro-ph.HE].
 - [123] G. A. Gomez-Vargas, M. A. Sanchez-Conde, J.-H. Huh, M. Peiro, F. Prada, A. Morselli, A. Klypin, D. G. Cerdeño, Y. Mambrini, and C. Muñoz, JCAP **1310**, 029 (2013), arXiv:1308.3515 [astro-ph.HE].
 - [124] S. Ando and E. Komatsu, Phys. Rev. **D87**, 123539 (2013), arXiv:1301.5901 [astro-ph.CO].
 - [125] A. X. Gonzalez-Morales, S. Profumo, and F. S. Queiroz, Phys. Rev. **D90**, 103508 (2014), arXiv:1406.2424 [astro-ph.HE].
 - [126] F. S. Queiroz and K. Sinha, Phys. Lett. **B735**, 69 (2014), arXiv:1404.1400 [hep-ph].
 - [127] S. Li, Y.-F. Liang, K.-K. Duan, Z.-Q. Shen, X. Huang, X. Li, Y.-Z. Fan, N.-H. Liao, L. Feng, and J. Chang, Phys. Rev. **D93**, 043518 (2016), arXiv:1511.09252 [astro-ph.HE].

- [128] Y. Mambrini, S. Profumo, and F. S. Queiroz, *Phys. Lett.* **B760**, 807 (2016), arXiv:1508.06635 [hep-ph].
- [129] A. Massari, E. Izaguirre, R. Essig, A. Albert, E. Bloom, and G. A. Gómez-Vargas, *Phys. Rev.* **D91**, 083539 (2015), arXiv:1503.07169 [hep-ph].
- [130] F. S. Queiroz, C. E. Yaguna, and C. Weniger, *JCAP* **1605**, 050 (2016), arXiv:1602.05966 [hep-ph].
- [131] S. Profumo, F. S. Queiroz, and C. E. Yaguna, *Mon. Not. Roy. Astron. Soc.* **461**, 3976 (2016), arXiv:1602.08501 [astro-ph.HE].
- [132] D. Q. Adams, L. Bergstrom, and D. Spolyar, (2016), arXiv:1606.09642 [astro-ph.CO].
- [133] S. Archambault *et al.* (VERITAS), *Phys. Rev.* **D95**, 082001 (2017), arXiv:1703.04937 [astro-ph.HE].
- [134] A. Khatun, R. Laha, and S. K. Agarwalla, (2017), arXiv:1703.10221 [hep-ph].
- [135] M. D. Campos, F. S. Queiroz, C. E. Yaguna, and C. Weniger, (2017), arXiv:1702.06145 [hep-ph].
- [136] I. Antoniadis, A. Boyarsky, S. Espahbodi, O. Ruchayskiy, and J. D. Wells, *Nucl. Phys.* **B824**, 296 (2010), arXiv:0901.0639 [hep-ph].
- [137] J. Bramante, R. S. Hundi, J. Kumar, A. Rajaraman, and D. Yaylali, *Phys. Rev.* **D84**, 115018 (2011), arXiv:1106.3819 [hep-ph].
- [138] J. Kumar, A. Rajaraman, and D. Yaylali, *Phys. Rev.* **D86**, 115019 (2012), arXiv:1209.5432 [hep-ph].
- [139] J. Kumar, A. Rajaraman, and J. D. Wells, *Phys. Rev.* **D77**, 066011 (2008), arXiv:0707.3488 [hep-ph].
- [140] E. C. G. Stueckelberg, *Helv. Phys. Acta* **11**, 225 (1938).
- [141] E. C. G. Stueckelberg, *Helv. Phys. Acta* **11**, 299 (1938).
- [142] B. Kors and P. Nath, *Phys. Lett.* **B586**, 366 (2004), arXiv:hep-ph/0402047 [hep-ph].
- [143] S. L. Adler, *Phys. Rev.* **177**, 2426 (1969).
- [144] J. S. Bell and R. Jackiw, *Nuovo Cim.* **A60**, 47 (1969).
- [145] A. Bilal, (2008), arXiv:0802.0634 [hep-th].
- [146] M. E. Peskin and D. V. Schroeder, *An Introduction to quantum field theory* (1995).